Anais da Academia Brasileira de Ciências (2014) 86(1): 85-116
(Annals of the Brazilian Academy of Sciences)
Printed version ISSN 0001-3765 / Online version ISSN 1678-2690
http://dx.doi.org/10.1590/0001-37652014108312
www.scielo.br/aabc

Geology, petrography and geochemistry of the A-type granites from the Morro Redondo Complex (PR-SC), southern Brazil, Graciosa Province

FREDERICO C.J. VILALVA[1] and SILVIO R.F. VLACH[2]

[1]Departamento de Geologia, Centro de Ciências Exatas e da Terra, Universidade Federal do Rio Grande do Norte, Campus Universitário Lagoa Nova, Caixa Postal 1639, 59078-970 Natal, RN, Brasil
[2]Departamento de Mineralogia e Geotectônica, Instituto de Geociências, Universidade de São Paulo, Rua do Lago, 562, Cidade Universitária, 05508-080 São Paulo, SP, Brasil

Manuscript received on July 23, 2012; accepted for publication on April 15, 2013

ABSTRACT

The Morro Redondo Complex is one of the most important occurrences of the Graciosa A-type Province, southern Brazil. It consists of the Papanduva and Quiriri granitic plutons and a contemporaneous bimodal volcanic association. The Papanduva Pluton includes massive and deformed peralkaline alkali-feldspar granites with Na-Ca and Na-amphiboles and clinopyroxenes. The deformed types are the most evolved rocks in the province and carry rare 'agpaitic' minerals, some being described for the first time in granites from Brazil. The larger Quiriri Pluton comprises massive, slightly peraluminous, biotite syeno- and monzogranites with rare Ca-amphibole. Biotite compositions are relatively homogeneous, whereas sodic amphiboles and clinopyroxenes show increasing Na and Fe^{3+} evolving paths. The Morro Redondo granites are ferroan, with high SiO_2, alkalis and HFSE contents; the peralkaline types registering the highest fe#. LILE and HFSE abundances increase with the agpaitic index and the most evolved are HHP granites, with radiogenic heat production up to 5.7 μWm^{-3}. Geothermobarometric estimates indicate emplacement under low pressures (~100 MPa), at temperatures up to 850-800 °C, and relatively reduced (QFM) and oxidized ($+1 < \Delta_{QFM} < +3$) environments for the Papanduva and Quiriri Plutons, respectively. In both cases, melts evolved to relatively high oxidation states upon crystallization progress.

Key words: A-type granites, geochemistry, petrography, Graciosa Province, mineralogy, Morro Redondo Complex.

INTRODUCTION

A-type magmatic provinces are widespread in the Earth's crust and have been formed since Archean times as a result of geodynamic processes associated to extensional tectonic environments. The diversity of rock types, with contrasting petrographic and geochemical signatures (e.g. Whalen et al. 1987, Eby 1992, Poitrasson et al. 1995, King et al. 1997, Schmitt et al. 2000, Litvinovsky et al. 2002, Gualda and Vlach 2007a, b, Nardi and Bitencourt 2009) is a particular feature of A-type magmatism. Although the nature of such diversity has been heavily discussed in literature, there is still no general consensus on the petrogenetic models and sources involved in their genesis (e.g. Martin 2006, Bonin 2007). The Graciosa Province, southern Brazil (Gualda and Vlach 2007a) is a typical example, where A-type granites and syenites from

Correspondence to: Frederico Castro Jobim Vilalva
E-mail: fredcjv@ufrnet.br

two contrasted petrographic associations, namely alkaline and aluminous (subalkaline), as well as related K-rich dioritic, gabbroic and some volcanic rocks were emplaced during the final stages of the Brasiliano/Pan-African Orogeny, at the end of the Neoproterozoic. Such diversity provides an ideal setting to investigate the evolution, composition and geotectonic significance of A-type granitoids and associated rocks (Gualda and Vlach 2007a, b, c, Vlach and Gualda 2007, Vlach et al. 2011).

The Morro Redondo Complex (Góis 1995) is one of the largest and most important occurrences of A-type granites in the Graciosa Province. It crops out close to the Atlantic coast line between the states of Paraná and Santa Catarina, southern Brazil, and is made of granitic rocks of both alkaline and aluminous petrographic associations, along with a coeval bimodal volcanic association. Such characteristics make the complex an interesting site to the study of the petrographic variability of A-type rocks and their genetic relationships. In this contribution, we present and discuss general geologic, petrographic, magnetic susceptibility, as well as mineral and whole-rock chemical data for the granites of the Morro Redondo Complex, aiming to improve the knowledge of these rocks, to compare results with the available data from other occurrences of the province, and to establish a solid background for petrological studies currently in progress on the genesis and evolution of the Morro Redondo Complex, as well as the Graciosa Province as a whole.

General Geology

The A-type Graciosa Province was formed during an extensional (post-collisional sensu Liégeois 1998) tectonic environment related to the Gondwana amalgamation in south-southeast Brazil, during the final stages of the Brasiliano/Pan-African Orogeny, at ca. 580 – 583 Ma (Vlach et al. 2011). The province encompasses several granitic and syenitic plutons, roughly circular to irregular in outline, intrusive into Archean and Neoproterozoic rocks of the Luiz Alves and Curitiba Microplates and the Paranaguá Terrain (Basei et al. 1992, Siga Jr et al. 1995), along an arc parallel to the present-day Atlantic coast line between the southeastern part of São Paulo and the northwestern portion of Santa Catarina states (Fig. 1a). Associated rocks include minor occurrences of K-rich diorites and gabbros, hybrid rocks and volcanics of a bimodal association. Contemporaneous volcano-sedimentary rocks are also described in the Campo Alegre, Guaratubinha and Corupá basins (Siga Jr et al. 2000, Almeida et al. 2012; Fig. 1a).

An important characteristic of the Graciosa Province is the coexistence of two distinct petrographic associations, either of alkaline or aluminous (subalkaline) affinity, which resemble many A-type provinces worldwide (e.g. Lameyre and Bowden 1982, Vlach et al. 1990, Pitcher 1993, Poitrasson et al. 1995, King et al. 1997, Litvinovsky et al. 2002, Qiu et al. 2004). The alkaline association is composed of metaluminous alkali-feldspar syenites to peralkaline hypersolvus granites, whereas the aluminous association comprises metaluminous to moderately peraluminous subsolvus syeno- and monzogranites. Detailed studies on the geology, petrography, mineralogy and geochemistry of the province can be found in Gualda and Vlach (2007a, b, c), Vlach and Gualda (2007) and references therein.

The Morro Redondo Complex

Since the pioneering works by Maack (1953) and Trein (1967), who introduced the term 'Morro Redondo Granite' in literature, several authors have contributed to the geology, structure, petrography, geochemistry and geochronology knowledge on the granitic and volcanic rocks constituted therein (e.g. Kaul 1984, 1997, Machado et al. 1993, Góis 1995, Kaul and Cordani 1994, 2000, Siga Jr et al. 1994). The term Morro Redondo Complex, used in agreement with ISSC (1987, see also Ulbrich et al. 2001), was coined by Góis (1995), taking into

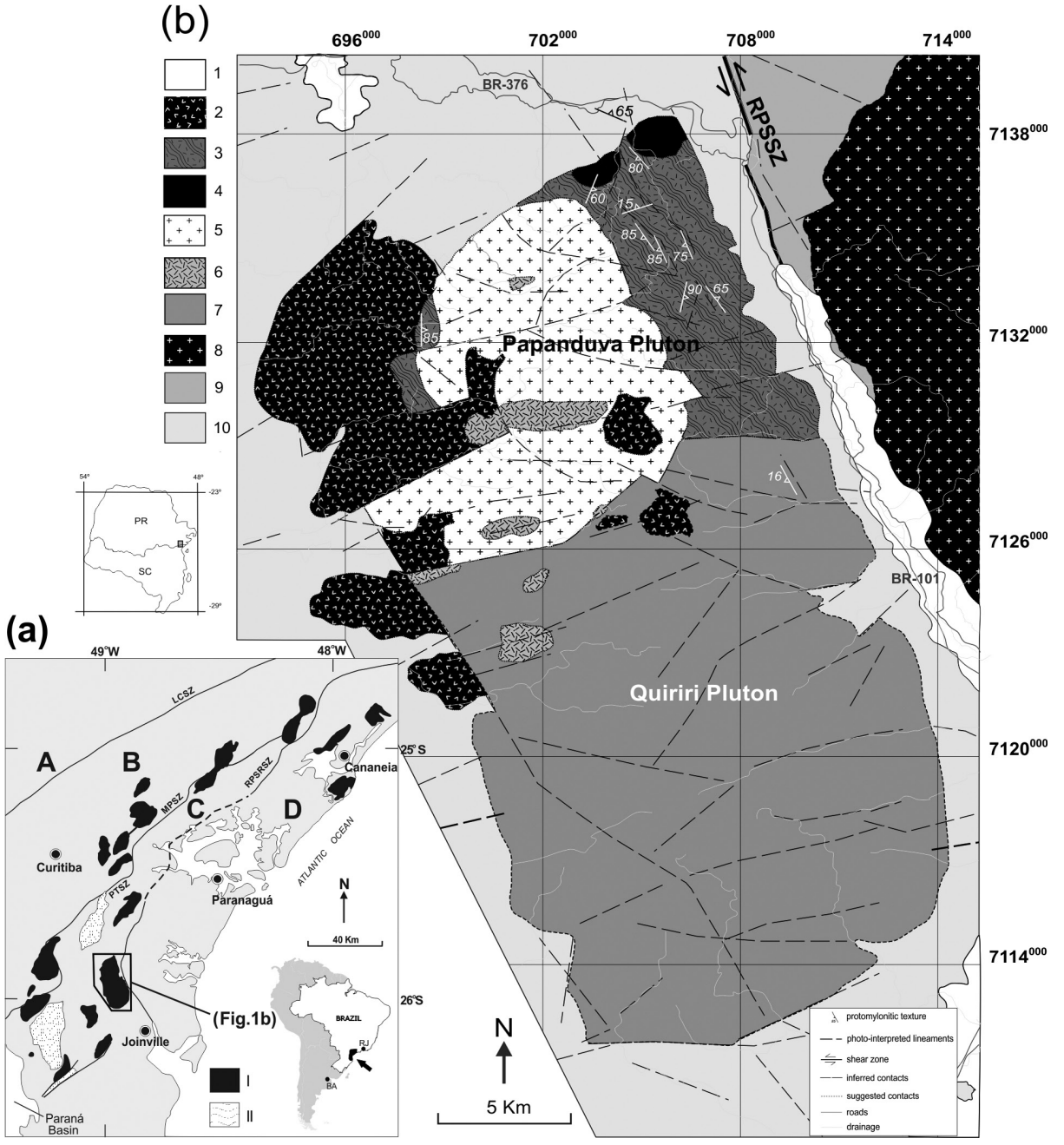

Figure 1 - Geological context of the Morro Redondo Complex. (a) Geological sketch of the Neoproterozoic A-type Graciosa Province (I) showing the location of the Morro Redondo Complex, as well as contemporaneous volcanosedimentary basins (II) in southern Brazil and the positioning in the South America Continent (RJ = Rio de Janeiro, BA = Buenos Aires, Argentina). Main regional tectonic units are: A – Ribeira Fold Belt, B – Curitiba Microplate, C – Luiz Alves Microplate (Craton), D – Paranaguá Terrain (Coastal Granitoid Belt). Adapted from Prazeres Filho et al. (2003) and Gualda and Vlach (2007a). (b) Geological map of the Morro Redondo Complex and surrounding areas. (1) alluvial-colluvial deposits, (2) contemporaneous bimodal volcanic rocks, (3 to 6) peralkaline alkali-feldspar granites from the Papanduva Pluton: (3) protomylonitic facies, (4) cataclastic facies, (5) massive facies, (6) microgranitic facies; (7) peraluminous biotite sieno - and monzogranites from the Quiriri Pluton, (8) Estrela high-K calc-alkaline granite and (9) metasedimentary rocks of the Paranaguá Terrain; (10) gneiss, granulites and migmatites of the Luiz Alves Microplate. Adapted from Vilalva (2007).

account the association of intrusive and extrusive rocks. Thereafter, Kaul (1997) subdivided the intrusive rocks into two major units, viz. Papanduva and Quiriri; the former constituted by peralkaline, the latter by slightly peraluminous granitic varieties. Here, we adopt the term *pluton* instead of *unit*, given that these units constitute structurally defined plutonic bodies, related to distinct intrusive events (cf. Ulbrich et al. 2001).

The Morro Redondo Complex extends to 25 km along N20°W and occupies ~250 km^2 between the cities of Tijucas do Sul and Garuva, states of Paraná and Santa Catarina, respectively, southern Brazil (Fig. 1b). It is intrusive into Archean granulites, gneisses and migmatites of the Luiz Alves Microplate. The eastern border is close to the N15° – 25°W trending Rio Palmital-Serrinha Shear Zone (RPSSZ), the main limit between the Archean rocks (to the west) and the Neoproterozoic granitoid rocks of the Paranaguá Domain (to the east; Fig. 1a).

Granitic exposures are characterized by mountains with elevations of up to 1,600 m, alternated with remains of eroded plateaus, while flatlands with elevations around 700 – 900 m define areas dominated by volcanic rocks (Fig. 2). Most of the outcrops are fairly weathered blocks and boulders, while expositions in mountain escarpments and waterfalls are scarce. Furthermore, these areas are covered by almost intact Atlantic Forest, with the exception of some parts in the western portion, where pines are exploited. Thick vegetation cover, rugged terrain and also very humid weather strongly limit access to the area and the sampling of fresh rocks, especially in the inner portions of the complex.

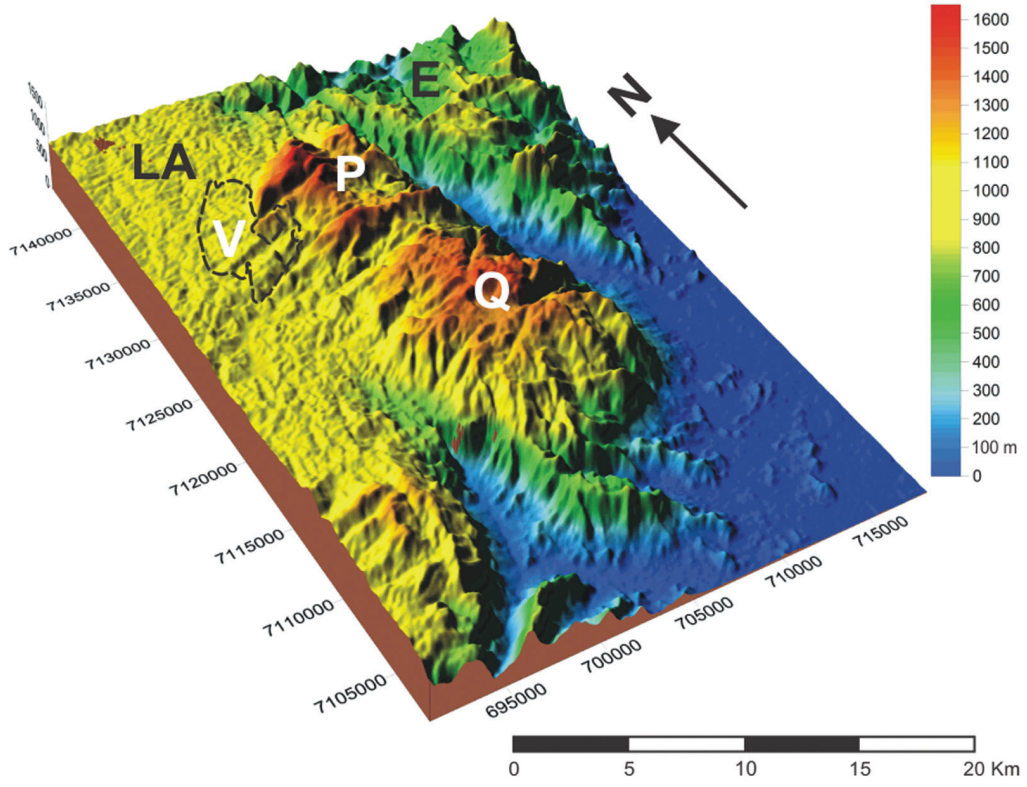

Figure 2 - SRTM 3D digital model for the Morro Redondo Complex and surrounding areas based on contour lines equidistant at 5 meters through mathematical interpolation using the software Global Mapper. **P**: Papanduva Pluton, **Q**: Quiriri Pluton, **V**: main outcrops of the associated bimodal volcanic rocks, **LA**: Luiz Alves Microplate, **E**: Estrela high-K calc-alkaline granite (Paranaguá Terrain).

Granitic rocks

Papanduva Pluton

The Papanduva Pluton crops out in the northern part of the complex, covering an area of ~60 km^2. It is made of leucocratic ($2 \leq M' \leq 9$), white to gray-colored, peralkaline granites grouped into four main petrographic facies by Vilalva (2007), as follows (Fig. 1b):

1. *Massive facies:* slightly inequigranular, coarse to medium-grained massive alkali-feldspar granite, with sodic-calcic and sodic amphibole and pyroxene (Fig. 3a). This is the main facies, identified in the central and southwest parts of the pluton. Centimetric to metric amphibole-bearing pegmatite veins, miarolitic cavities and vugs and centimetric astrophyllite-bearing microgranular mafic enclaves are occasional.
2. *Deformed 'protomylonitic' facies*: alkali-feldspar granites showing well-marked sub-magmatic (cf. Blenkinsop 2000), close-to-solidus deformational structures which trend N30°W/80°SW and N15°E/70°SE along to the Papanduva Pluton borders. Here, mineral fabrics give the granites a protomylonitic (and sometimes porphyroclastic) appearance, with deformed and oriented sodic amphibole (up to 0.5 cm), alkali-feldspar and some quartz megacrysts, in a fine-grained saccharoidal matrix, which often displays whitish to yellowish rare minerals (Fig. 3b). Miaroles and vugs are locally seen.
3. *Deformed 'cataclastic' facies*: slightly sub-magmatic deformed, coarse to medium-grained, dark colored alkali-feldspar granites with prismatic crystals and radiating aggregates of pyroxene as the main mafic phase (Fig. 3c). It was mapped only at the northernmost portion of the pluton.
4. *Microgranitic facies*: slightly inequigranular fine-grained alkali-feldspar microgranites, eventually with planar flow structures defined by euhedral amphibole crystals (Fig. 3d). They appear as centimetric to decametric dikes and other minor bodies which intrude the main granites of both the Papanduva and Quiriri plutons.

Quiriri Pluton

The largest Quiriri Pluton occupies the central and southern parts of the complex, covering an area of ~190 km^2 (Fig. 1b). It is mainly composed of gray to red-colored biotite granites ($2 \leq M' \leq 9$) with well-developed quartz crystals. Distinct textural varieties were identified, but they could not be mapped properly due to the poor quality of outcrops and difficult accesses. The main facies, here named *Q1*, is widespread in the whole pluton. Granites show massive structures and reddish, inequigranular, medium-grained textures (Fig. 4a). Alkali feldspar forms larger, red-stained, tabular crystals and dominates over whitish tabular plagioclase. Incipient magmatic flow structures and rapakivi-like textures are rarely seen. A similar variety, *Q2*, with typical gray colors (Fig. 4b), locally amphibole-bearing, appears close to the northwestern portion, while a third, red-colored, relatively plagioclase-poor facies crops out in the central area and locally in the northeastern part. It was named *Q3* and carries primary biotite partially to completely replaced by chlorite and other hydrothermal minerals (Fig. 4c). Minor bodies and dikes of granite-porphyries with alkali-feldspar, plagioclase and quartz phenocrysts (up to 1.2 cm, cf. Fig. 4d) in a fine-grained matrix appear in some outcrops in the northwestern and northeastern areas. These are identified as *Q4* facies.

Granophiric intergrowths can be seen under hand lenses in some varieties of the Q3 and Q4 facies, while miarolitic cavities and vugs are ubiquitous. Simple pegmatite pods, aplite veins, as well as microgranular enclaves and both mafic and felsic *schlieren*-like structures, are typical of the main Q1 facies. Enclaves include typical felsic and

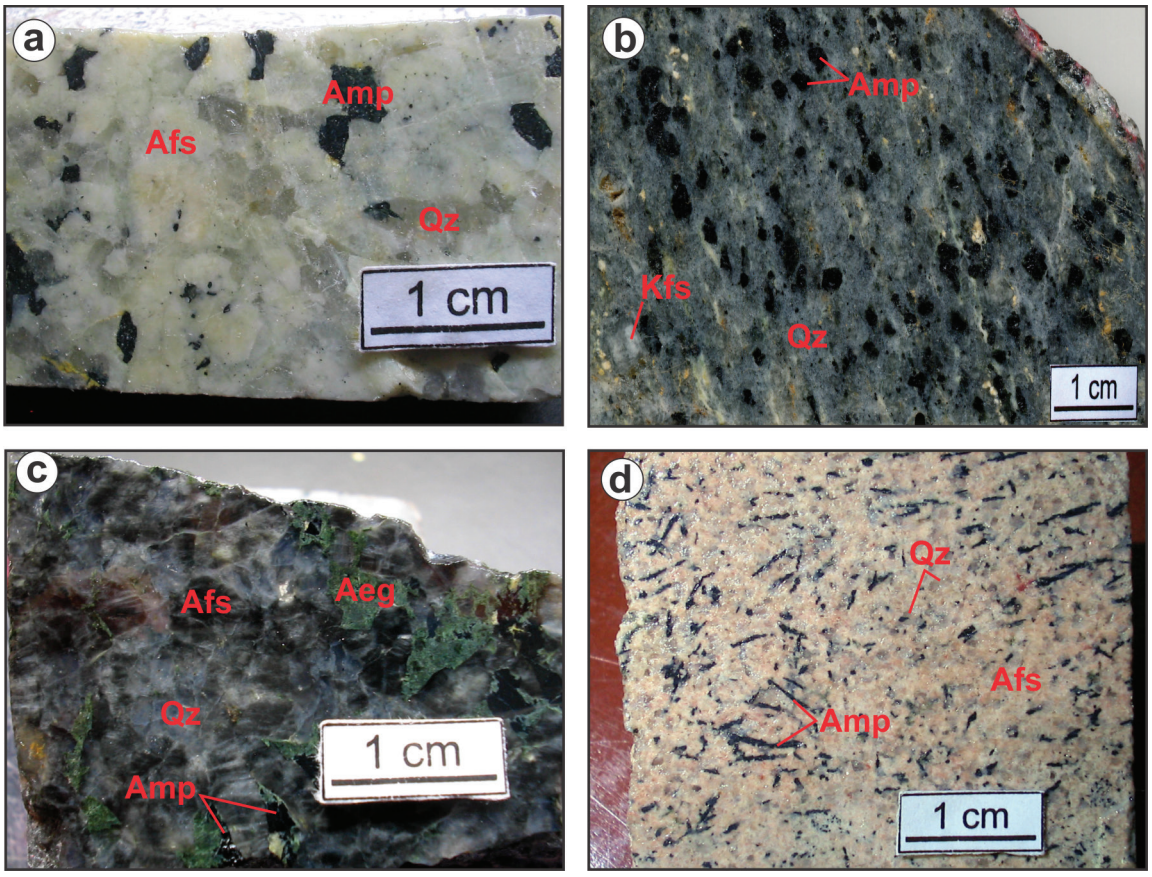

Figure 3 - Petrographic features of the Papanduva Pluton. **(a)** Macroscopic aspect of hololeucocratic alkali-feldspar granite of the massive facies. The medium-grained equigranular texture is defined by alkali feldspar (Afs), quartz (Qz) and sodic-calcic amphibole (Amp) as the main mafic phase. **(b)** Macroscopic aspect of alkali-feldspar granite of the deformed 'protomylonitic' facies, with elongated and rounded sodic amphibole megacrysts (Amp) in a fine-grained matrix made of quartz (Qz) and potassic feldspar (Kfs). **(c)** Macroscopic aspect of alkali feldspar granite of the deformed 'cataclastic' facies. The medium-grained equigranular texture is characterized by deformed quartz (Qz) and alkali feldspar (Afs) crystals and interstitial aegirine (Aeg) and sodic amphibole (Amp). **(d)** Macroscopic aspect of leucocratic alkali feldspar microgranite of the microgranitic facies, with magmatic flow texture defined by oriented prismatic sodic amphibole crystals (Amp) among alkali feldspar (Afs) and quartz (Qz).

mafic fine-grained varieties of granitic (Fig. 4e) and dioritic compositions, respectively, and medium to fine-grained leucocratic varieties with plagioclase and interstitial mafic minerals similar to those found in the host granite (Fig. 4f).

Volcanic and subvolcanic rocks

Volcanic rocks occupy ~40 km^2 in the northwestern and central areas of the complex (Figs. 1b and 2). General geologic and petrographic data are presented by Góis (1995) and Kaul (1997). Lithotypes are mainly porphyritic and microporphyritic rhyolites and alkali-feldspar rhyolites, with infrequent well-developed flow structures. They are peralkaline, with Na-Ca and Na-clinopyroxenes and amphiboles. A local occurrence of alkali-feldspar rhyolite with aenigmatite as flow-oriented microphenocrysts was found in the northwesternmost area. Thin basaltic flows occur between the rhyolite layers. These basalts are made of plagioclase (andesine-labradorite), augite, pigeonite (sometimes as cores in augite), apatite, magnetite and ilmenite and show intergranular to

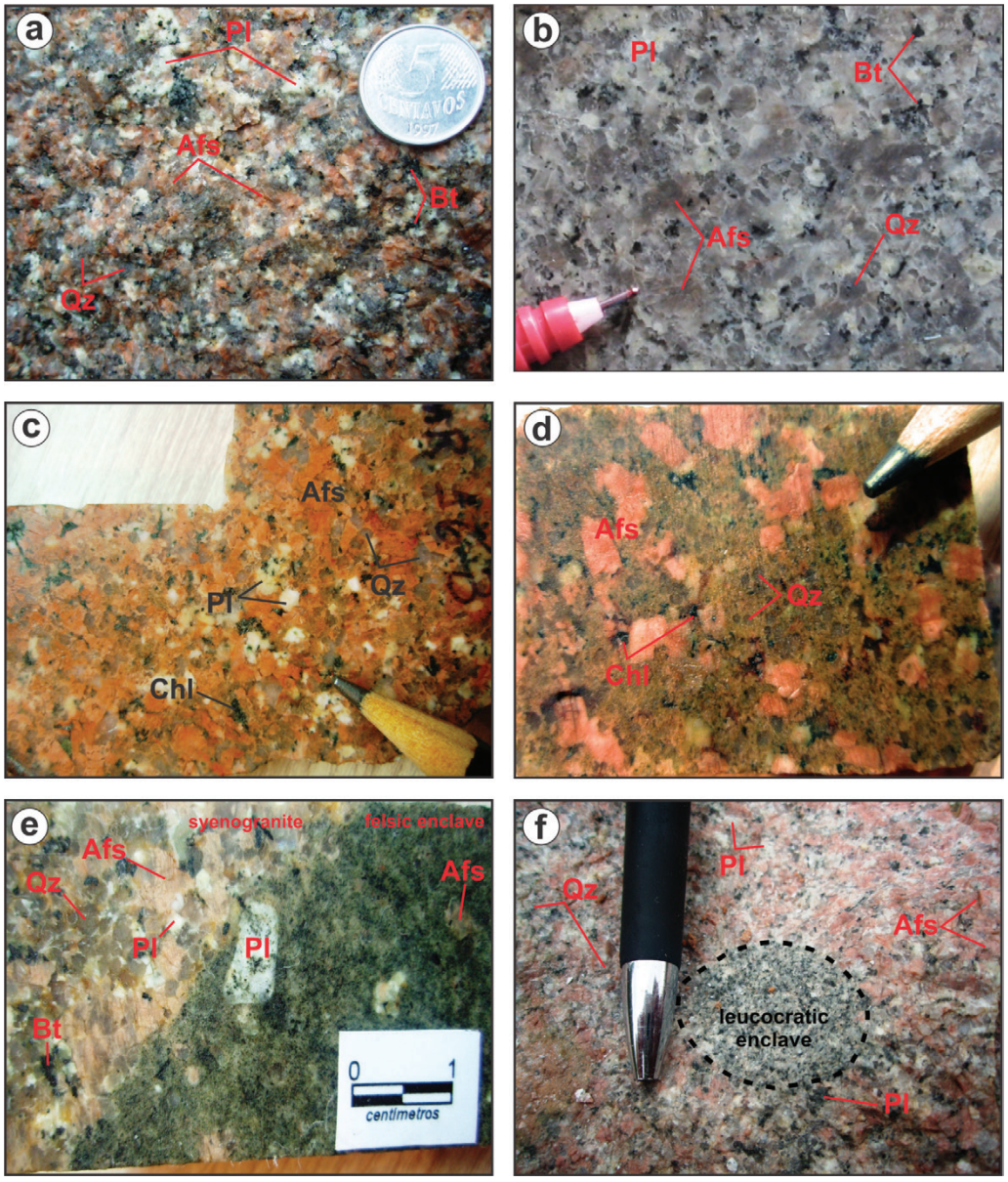

Figure 4 - Petrographic aspects of the Quiriri Pluton. **(a)** Massive, medium-grained, hololeucocratic, red-colored syenogranite of the Q1 facies, showing equi to inequigranular texture defined by quartz (Qz), plagioclase (Pl) and red-clouded alkali feldspar crystals (Afs), as well as biotite (Bt) as the main mafic mineral. **(b)** Massive, medium-grained, hololeucocratic, gray-colored syenogranite of Q2 facies. The inequigranular texture is defined by red to gray-colored alkali feldspar (Afs), minor plagioclase (Pl) and quartz (Qz) crystals and interstitial biotite (Bt). **(c)** Massive, medium to coarse grained, plagioclase-poor, hololeucocratic, red-colored syenogranite of Q3 facies. Large red-clouded alkali feldspar crystals (Afs) and minor quartz (Qz), plagioclase (Pl) and chlorite (Chl) pseudomorphs after biotite define an inequigranular texture. **(d)** Porphyritic syenogranite of Q4 facies showing tabular alkali feldspar (Afs) and globular quartz megacrysts (Qz) in a fine-grained matrix of poikilitic quartz enclosing plagioclase, chlorite (Chl) pseudomorphs after biotite and some late alkali feldspar crystals. **(e)** Detail of microgranular felsic enclave (right) composed of quartz, feldspars and chlorite pseudomorphs after biotite. Note euhedral plagioclase (Pl) and alkali feldspar (Afs) megacrysts that could represent xenocrysts from the syenogranite of Q1 facies (left) containing alkali feldspar (Afs), quartz (Qz), plagioclase (Pl) and biotite (Bt) in a inequigranular texture. **(f)** Detail of leucocratic enclave displaying mainly plagioclase and interstitial chlorite and epidote (dark colors) replacing primary biotite, within the inequigranular, red-colored inequigranular Q1 syenogranite showing alkali feldspar (Afs), plagioclase (Pl), quartz (Qz) and interstitial biotite (Bt).

subophitic textures. Interstitial microgranophyric intergrowths and chlorite, biotite and Ca-amphibole pseudomorphs after pyroxene are sometimes recognized. Afanitic to porphyritic andesites and andesi-basalts with plagioclase (oligoclase-andesine), augite, biotite, magnetite, ilmenite and some quartz appear in very few outcrops.

Centimetric to metric basic dikes cross cut the Quiriri granites. Despite the fewness of field relationships, most of them appear to belong to the young Mesozoic (NW-SE and NE-SW) dike swarms of the Paraná Triple Junction (Coutinho 2008), nevertheless a few others appear to be syn-plutonic dikes.

Cross-cutting relationships and sequence of the magmatic events

Field structural relationships among the studied facies are very scarce and, therefore, the stratigraphy of the magmatic events is still a matter of debate. Rhyolite xenoliths are observed in the Papanduva main massive granites, while related peralkaline microgranitic dikes cut the Quiriri biotite granites. Such evidences suggest the main volcanism episode preceded, to some extent, the emplacement of the Papanduva main granites, whereas the late peralkaline microgranitic varieties were emplaced later than the Quiriri biotite granites. Nevertheless, it must be remembered that the building of a pluton may be very complex, involving the emplacement of several batches of magmas with contrasted rheological properties. Thus, the available information is not sufficient to draw a reliable scenario.

MATERIALS AND METHODS

This work presents, besides conventional field and petrographic data, magnetic susceptibility (MS) and mineral and whole-rock chemical data obtained from the intrusive rocks of the Morro Redondo Complex at the facilities of the Núcleo de Apoio à Pesquisa (NAP) GeoAnalítica-USP, Universidade de São Paulo, Brazil.

MS measurements were made with the GM Instruments SM-20 Portable Susceptibilimeter, considering a mean of 10 measurements per sample taken in appropriate outcrops during the field work and in rock slabs afterwards.

Mineral compositions were obtained by Wavelength Dispersive Spectrometry (WDS) microanalyses using a JEOL JXA-8600S Electron Microprobe under operating conditions of 15 kV and 20 nA for the column acceleration voltage and beam current. Pyroxenes, amphiboles, biotite, alkali feldspar and plagioclase were analyzed following the procedures described in Gualda and Vlach (2007b). The PROZA software (e.g. Bastin and Heijligers 1990) was employed for matrix effects corrections and data reduction. Mineral formulae and estimates of Fe^{2+}/Fe^{3+} ratios were calculated with the Mincal software (G.A.R. Gualda and S.R.F. Vlach, unpublished data, see also Deer et al. 1992, Droop 1987). Amphibole nomenclature follows Leake et al. (1997, 2004); Fe^{2+} and Fe^{3+} were estimated with a variant of the method by Schumacher (1997), as discussed in Gualda and Vlach (2005). Clinopyroxene was classified according to Morimoto et al. (1988).

Whole-rock chemical analyses were determined using Inductively Coupled Plasma Atomic Emission Spectrometry/Mass Spectrometry (ICP-AES/MS) and X-Ray Fluorescence (XRF) instruments: major, minor and some trace-elements were quantified by ICP-AES and XRF, while most trace-elements were measured by ICP-MS, following the analytical protocols described by Mori et al. (1999) and Navarro et al. (2008), respectively. Radiogenic heat production per volume (**A**) was calculated using Th and U contents measured from the ICP-MS, after Rybach (1988):

$$\mathbf{A}\ (\mu Wm^{-3}) = 10^{-2} * \rho * [3.48 * K_2O + 2.56 * Th + 9.52 * U]$$

where K_2O is given in wt. % and Th and U in ppm. A medium rock density (ρ) of 2.70 g/cm^3 was adopted.

RESULTS

Petrography

Representative quantitative modal data for the granites are presented in Fig. 5. The Papanduva and Quiriri plutons are made of *hypersolvus* alkali-feldspar granites and *subsolvus* syenogranites, respectively. Moreover, a felsic microgranular enclave from the Quiriri Pluton plots as a monzogranite. Brief petrographic descriptions of these rocks are given below; additional microstructural relationships among the main rock-forming minerals will be presented in the mineralogical section.

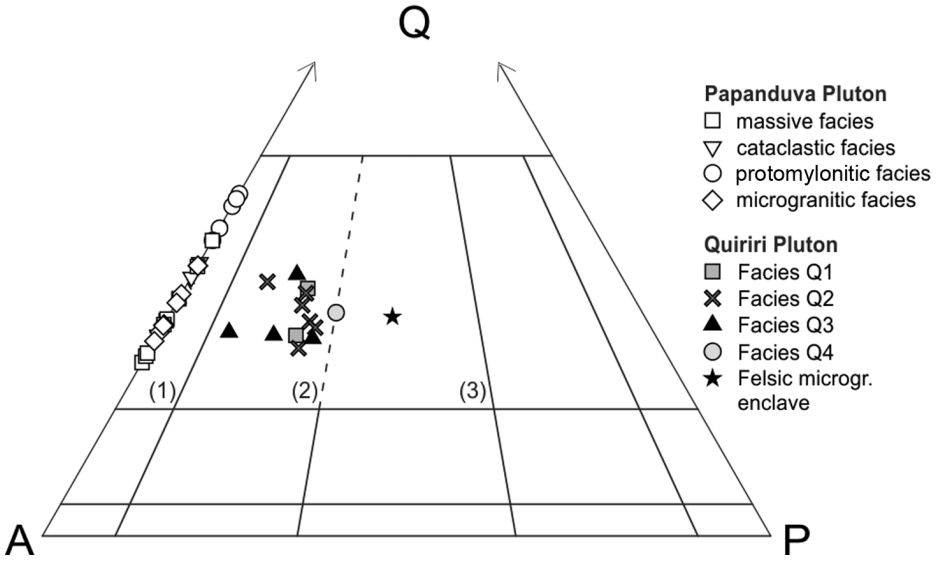

Figure 5 - Modal Quartz **(Q)** - Alkali Feldspar **(F)** - Plagioclase **(P)** diagram for oversaturated plutonic rocks according to Streckeisen (1976) showing compositional variations registered for the Papanduva and Quiriri Plutons, Morro Redondo Complex. Labeled fields are: **(1)** alkali-feldspar granite; **(2)** syenogranite and **(3)** monzogranite.

Papanduva Pluton

The texture of the main massive facies is characterized by large tabular crystals of mesoperthitic alkali feldspar with well-developed quartz; amphiboles and pyroxene are interstitial and homogeneously distributed (Fig. 6a). Two contrasted amphibole generations are identified: an early-crystallizing green Na-Ca amphibole, which corresponds to the main mafic phase and a late-crystallizing blue Na-amphibole as interstitial isolated crystals and overgrowths. Also a late-crystallizing phase, compositionally zoned Na-clinopyroxene appears as interstitial isolated euhedral crystals, fibro-radiated aggregates, and as ubiquitous mantles around amphibole. Zircon, chevkinite, fluorite, astrophyllite and some ilmenite, magnetite and titanite are accessory minerals.

Rare microgranular mafic enclaves contain euhedral to subhedral quartz and alkali feldspar megacrysts immersed in a fine-grained, hypidiomorphic to xenomorphic quartz-feldspathic matrix with Ca-amphibole, apatite and astrophyllite.

Distinct deformational textures characterize the 'protomylonitic' and 'cataclastic' facies. Of importance, several of the observed textures depicted below suggest that deformation occurred mostly under sub-magmatic conditions, i.e. involving flow of melting and crystal mushes, assisted by crystal plastic deformation (Blenkinsop 2000, Passchier and Trouw 2005), rather than in solid-state conditions.

The deformed 'protomylonitic' facies shows textures defined by oriented and deformed ellipsoidal to irregular Na-amphibole, perthitic alkali feldspar and minor quartz megacrysts (2.0 – 4.0 mm), the first displaying compositional zoning and the last undulose extinction. They are surrounded by a fine-grained, saccharoidal matrix made of recrystallized quartz, slightly perthitic microcline and albite, joined by Na-clinopyroxene and accessory minerals (Fig. 6b). On the other hand, in the deformed 'cataclastic' facies, interstitial and deformed Na-clinopyroxene and amphibole crystals, coarse quartz surrounded by fine recrystallized grains, crystal microfractures (mainly in coarse alkali feldspar and quartz) filled by fine-grained, late-crystallizing aggregates of quartz and feldspar, along with bent mesophertitic alkali feldspar crystals are typical features (Fig. 6c). Fluorite, astrophyllite, titanite, aenigmatite and some ilmenite are common accessory minerals in both facies. Zircon and late magnetite appear only in the deformed 'cataclastic' facies, while combinations of late to post-magmatic 'agpaitic' Ti-, Zr-, and REE-bearing rare silicates and oxides, such as narsarsukite, neptunite, elpidite and other (Na,K)-zirconosilicates, britholite, turkestanite, nacareniobsite, brookite and some as-yet unidentified minerals, are widespread in the deformed 'protomylonitic' facies, even in miarolitic cavities and vugs (Vilalva and Vlach 2010, Vilalva et al. 2013, Vlach and Vilalva 2007).

The microgranitic facies comprises equi to inequigranular fine-grained rocks with magmatic flow structures defined by prismatic Na-amphibole. These microgranites are characterized by abundant micrographic intergrowths of multiple morphologies (Fig. 6d). Main mafic minerals are Na-amphibole and/or Na-clinopyroxene, whereas chevkinite, fluorite, post-magmatic (Mn, Zn)-rich ilmenite (Vilalva and Vlach 2009) and zircon are accessory minerals.

Quiriri Pluton

The granites of the Quiriri Pluton have variable quantities of perthitic alkali feldspar, quartz and sodic plagioclase (oligoclase) with allanite, titanite, fluorite, zircon, apatite, magnetite and ilmenite as accessory minerals. The most typical Q1, as well as the Q2 facies, display equi to inequigranular hypidiomorphic textures defined by slightly larger tabular alkali feldspar crystals, deformed quartz with undulose extinction and deformation lamellae, plagioclase, and interstitial biotite (Figs. 7a, b). Ca-amphibole is occasional in the grayish variety. The most contrasted varieties are alkali-feldspar granites of the Q3 facies, with numerous granophyric intergrowths in the matrix (Fig. 7c), and porphyritic syenogranites (granite porphyries) of the Q4 facies, with perthitic alkali feldspar, minor sodic plagioclase, and quartz megacrysts in a fine-grained quartz-feldspatic matrix containing biotite, zircon, magnetite, ilmenite, apatite and allanite (Fig. 7d).

Hydrothermal alteration is ubiquitous in all petrographic facies except the grayish Q2 (Fig. 4). Related textures include: biotite crystals replaced by chlorite + epidote + magnetite; post-magmatic albite filling interstices between alkali feldspar crystals or as partial rims around plagioclase; sericitic or saussuritic plagioclase; and sericitic, red-clouded alkali feldspar (e.g. Figs. 4c, d). The red-clouding phenomenon in feldspars occurs due to the precipitation of rosettes and needles of hematite from hydrothermal fluids into micro pores in the alkali feldspar surface, as a result of sub-solidus mineral–fluid replacement processes (e.g. Putnis et al. 2007). Indeed, in many outcrops, granite boulders show the red-staining concentrated in specific areas, which are always associated with epidote-filled microfractures.

Typical microgranular felsic enclaves are monzogranites with quartz, feldspars and chlorite pseudomorphs after biotite. Euhedral alkali feldspar, rounded quartz and minor plagioclase megacrysts, arguably xenocrysts from the host granite, are common (Fig. 7e). On the other hand, mafic microgranular enclaves are quartz-monzodiorites with biotite as the main mafic mineral, together with apatite, magnetite,

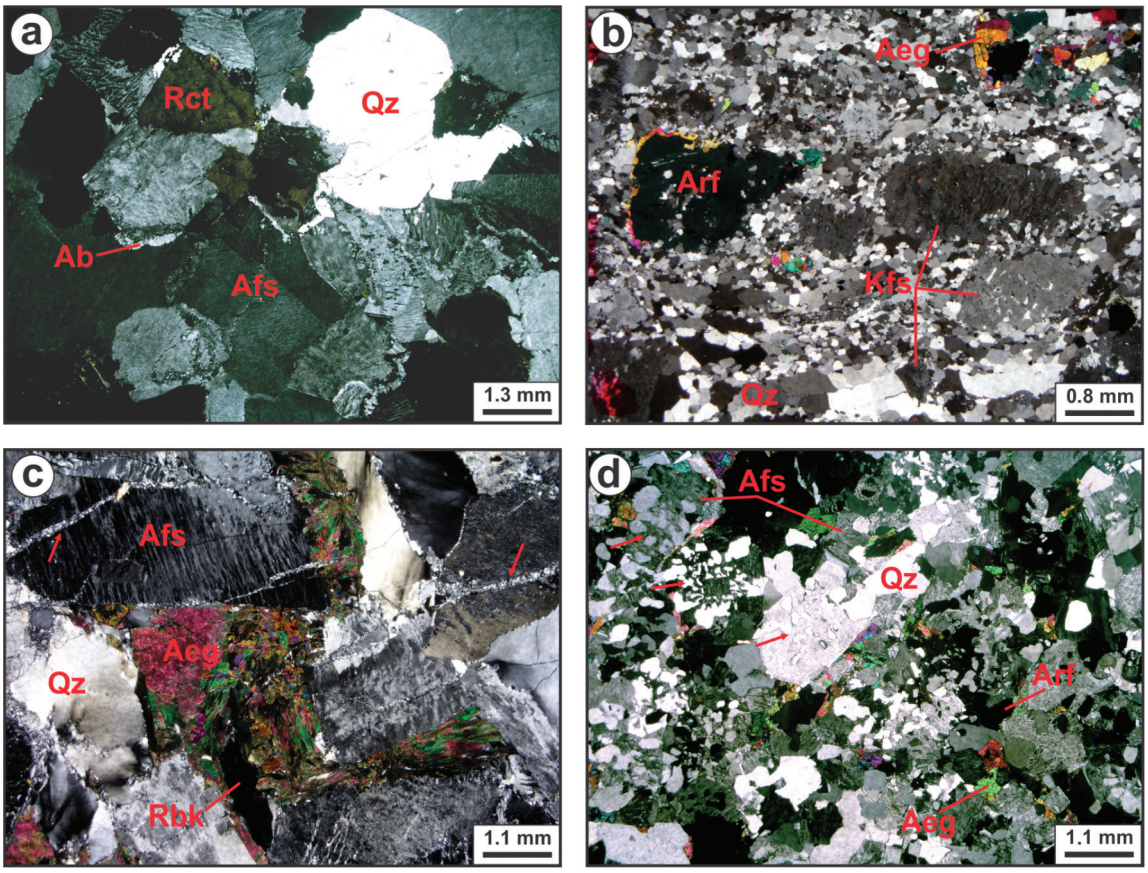

Figure 6 - Microtextural features of the Papanduva Pluton. **(a)** Textural aspect of alkali feldspar granite of the massive facies showing equi to inequigranular texture with tabular mesoperthitic alkali feldspar crystals (Afs), sometimes with albitic rims (Ab), as well as quartz (Qz) and interstitial ferrorichterite (Rct) crystals. **(b)** Textural aspect of alkali-feldspar granite of the deformed 'protomylonitic' facies, with potassic feldspar (Kfs) and arfvedsonite (Arf) porphyroclasts, the latter mantled by aegirine (Aeg), in a fine-grained recrystallized matrix of quartz (Qz), post-magmatic albite and potassic feldspar (Kfs). **(c)** Textural aspect of alkali feldspar granite of the deformed 'cataclastic' facies, with subhedral, perthitic to mesoperthitic alkali feldspar (Afs), quartz with undulose extinction (Qz) and interstitial aggregates of aegirine (Aeg), as well as some riebeckite (Rbk). Note recrystallized fine-grained quartz filling fractures in feldspar (arrows). **(d)** Textural aspect of alkali-feldspar microgranite of the microgranitic facies with equi to inequigranular texture defined by tabular alkali feldspar crystals (Afs) with interstitial quartz (Qz), aegirine (Aeg) and arfvedsonite (Arf). Graphic intergrowths between quartz and alkali feldspar are common (arrows). Photomicrographs with crossed polarizers.

and ilmenite. Leucocratic microgranular enclaves are made mainly (up to 80% volume) of euhedral tabular plagioclase (andesine). Interstitial chlorite, epidote, fluorite, titanite and magnetite have totally replaced the primary biotite and/or amphibole (Fig. 7f).

Magnetic Susceptibilities

Magnetic susceptibility measurement results are displayed as histograms in Fig. 8. Most values obtained for the Papanduva Pluton are lower than 1.0 x 10^{-3} SI, with a mean and mode values of 0.42 x 10^{-3} and 0.1 x 10^{-3} SI (Fig. 8a). Exceptions are some samples from the deformed 'cataclastic' facies that yield values as high as 6.0 x 10^{-3} SI, due to the presence of almost pure post-magmatic magnetite in micro-fractures or around Na- amphibole and pyroxene. Conversely, the Quiriri Pluton, albeit for some few measurements down to 0.04 x 10^{-3} SI (Q2 facies), registers mean

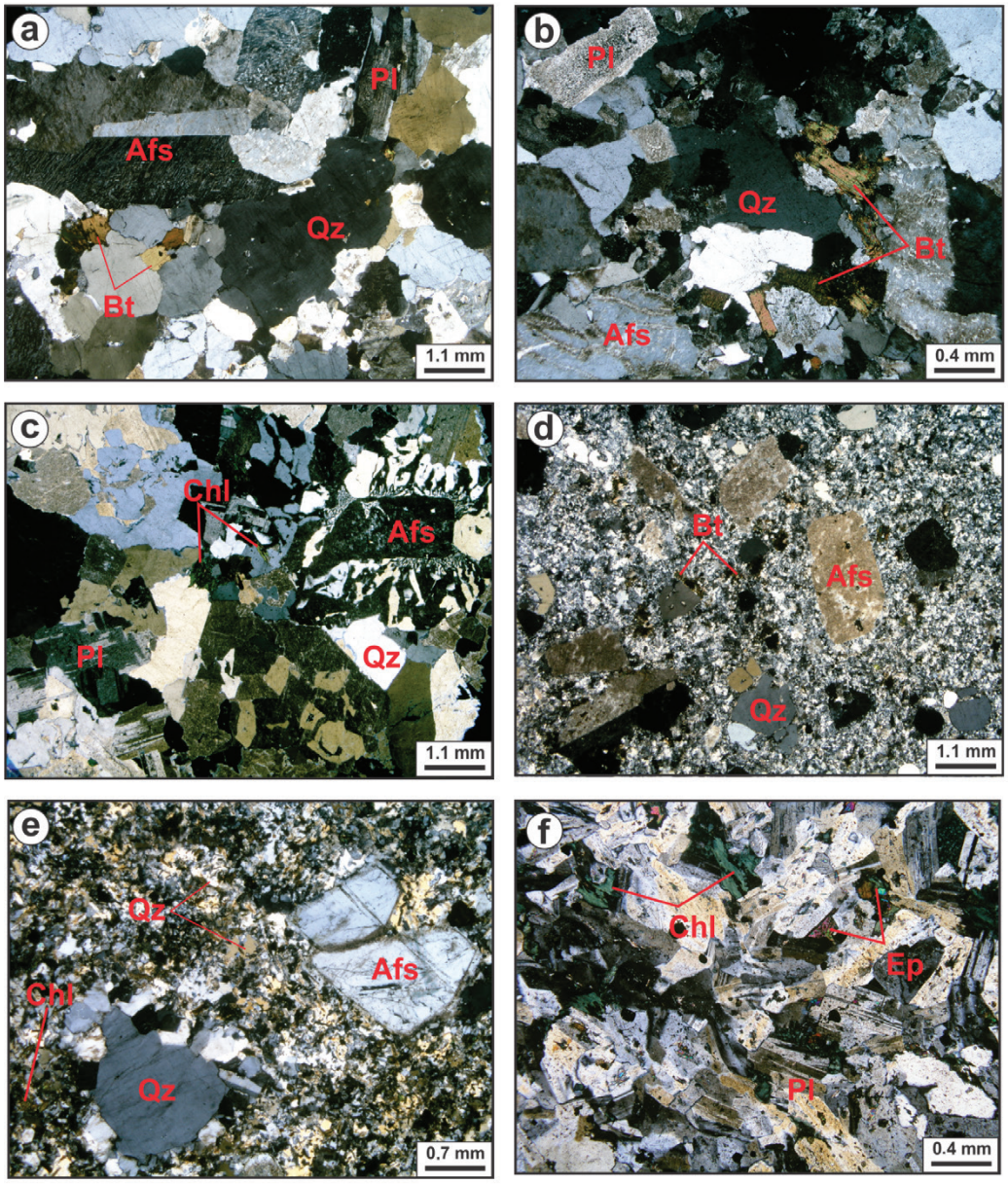

Figure 7 - Microtextural features of the Quiriri Pluton. **(a)** Textural aspect of massive, medium-grained inequigranular syenogranite of Q1 facies with slightly larger pertitic alkali feldspar crystals (Afs) and minor plagioclase (Pl), quartz (Qz) and interstitial biotite (Bt) crystals. **(b)** Textural aspect of massive, fine to medium-grained syenogranite of Q2 facies showing equi to inequigranular texture made of slightly larger alkali feldspar (Afs) and quartz (Qz) crystals, minor saussuritic plagioclase (Pl) and euhedral biotite. **(c)** Textural aspect of massive, medium grained, plagioclase-poor syenogranite of Q3 facies, with a inequigranular texture defined by alkali feldspar crystals (Afs) in granophyric intergrowths with quartz (Qz), scarce plagioclase (Pl) and interstitial chlorite (Chl) pseudomorphs after biotite. **(d)** Textural aspect of porphyritic syenogranite (granite porphyry) of Q4 facies with sericitic and red-clouded alkali feldspar (Afs) and globular quartz (Qz) megacrysts in a fine-grained quartz-feldspatic matrix with chlorite (Chl) pseudomorphs after biotite. **(e)** Textural detail of microgranular monzogranitic enclave within syenogranite of Q1 facies showing euhedral alkali feldspar (Afs) and globular quartz (Qz) megacrysts (xenocrysts?) in a fine-grained matrix of poikilitic quartz (Qz), minor plagioclase, some alkali feldspar and chlorite (Chl) pseudomorphs after biotite. **(f)** Detail of leucocratic enclave within syenogranite of Q1 facies, made essentially of euhedral plagioclase crystals (Pl), as well as chlorite (Chl) and epidote (ep) pseudomorphs after biotite and/or amphibole. Photomicrographs with crossed polarizers.

and mode values of 2.57 x 10^{-3} and 2.3 x 10^{-3} SI (Fig. 8b), up to 5-fold higher than those obtained for the Papanduva Pluton, as expected from their modal primary magnetite content.

The MS values of the peralkaline rocks from the Papanduva Pluton are amongst the lowest ever registered for rocks from the alkaline association within the Graciosa Province (typical values around 1.0 x 10^{-3} SI). In contrast, values for Quiriri samples, as well as their range of variation, are very similar to those measured in the aluminous association elsewhere within the province (cf. Gualda and Vlach 2007a).

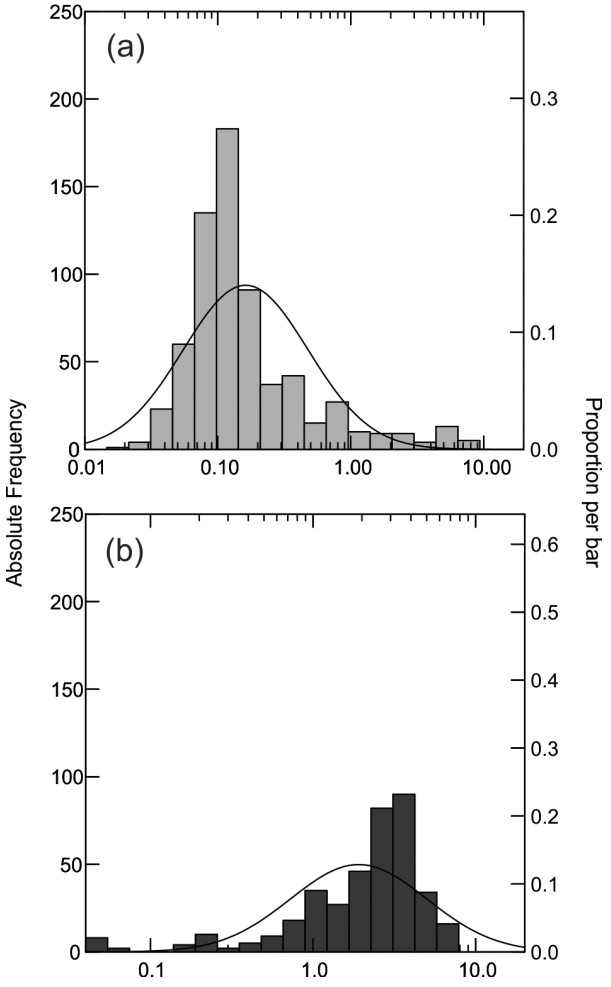

Figure 8 - Histograms (absolute frequency) showing the magnetic susceptibility (MS) variation for representative samples of the Papanduva **(a)** and Quiriri **(b)** Plutons.

MINERALOGY

General microstructure and chemistry of the main granite-forming minerals are presented below. Representative chemical compositions of feldspars, amphiboles, clinopyroxenes and biotite are given in Table I.

Alkali Feldspar

Alkali feldspar from the Papanduva Pluton forms mesoperthitic, euhedral to subhedral crystals in the massive and microgranitic facies, and slightly perthitic megacrysts and fine-grained microcline in the deformed 'protomylonitic' and 'cataclastic' facies. Integrated compositions of mesoperthitic crystals and perthitic megacrysts, which should approach primary compositions, vary between $Ab_{35-66}An_{0-1}Or_{65-34}$ and $Ab_{2-15}An_0Or_{99-85}$, respectively (Fig. 9). They are slightly enriched in Fe^{3+} when compared to alkali feldspars of peralkaline rocks from the Serra da Graciosa region within the province (Gualda and Vlach 2007b). Late to post-magmatic albite is also observed as interstitial pristine crystals or as swapped-rims around alkali feldspars in most samples. In the deformed 'protomylonitic' and 'cataclastic' facies, albite appears as granoblastic crystals in the matrix, as well as euhedral laths forming intergrowths with mafic minerals, which resemble the *khybinitic* texture of some undersaturated alkaline rocks (e.g. Gerasimovsky et al. 1974). In both cases, compositions are close to the ideal end-member ($Ab_{99-100}An_{0-0.1}Or_{1-0}$, cf. Table I, Fig. 9), but the laths register slightly higher Fe^{3+} contents (up to 1.7 wt. % Fe_2O_3) than the most typical post-magmatic albite crystals (up to 1.3 wt. % Fe_2O_3).

Alkali-feldspar from the Quiriri samples crystallizes as perthitic, euhedral to subheudral crystals, with well-developed chessboard textures. Their compositions vary around $Ab_{26-41}An_{0-1}Or_{74-58}$ (Table I, Fig. 9), and are similar to those observed in other plutons of the aluminous association elsewhere within the Graciosa Province (Gualda

TABLE I

Typical WDS analyses (wt. %) of alkali feldspar, albite, plagioclase, amphiboles, clinopyroxenes and biotite in granites of the Papanduva and Quiriri plutons, Morro Redondo Complex. Analyses of alkali feldspar from sample MR-19B refers to integrated perthitic compositions. Protomyl.: protomylonitic facies; Catacl.: cataclastic facies. Point_ID: analytical spot identification, c: core, i: intermediate, r: rim; b.d.l. = below detection limit; (-) = not analyzed; ferrohbl = ferrohornblende; ferroricht = ferrorichterite; arfv = arfvedsonite; rieb = riebeckite; aeg-aug = aegirine-augite.

Mineral	alkali feldspar				albite		plagioclase		ferrohbl	ferroricht	arfv	rieb	aeg-aug	aegirine		biotite	
Pluton	Papanduva		Quiriri		Papanduva		Quiriri		Quiriri	Papanduva			Papanduva			Quiriri	
Facies	Massive	Protomyl.	Q2	Enclave	Protomyl.		Q2	Enclave	Q2	Massive	Protomyl.	Catacl.	Massive	Protomyl.		Q2	
Sample	MR-39	MR-02A	MR-19B	MR-201B	MR-01A	MR-61	MR-19B	MR-201B	MR-15C	MR-39	MR-50(2)	MR-11 (A)	MR-121	MR-41	MR-06	MR-186A	MR-193
Cristal	1	1	1	4	1	2	1	7	1	5	1	1	1	1	6	1	1
Point_ID	p.1_c	p.1_c	p.1_c	p.2_i	p.1_c	p.2_r	p.3_c	p.2_i	p.2_c	p.2_c	p.1_r	p.1_r	p.1_r	p.4_c	p.1_r	p.1_c	p.1_r
SiO_2	66.53	64.55	64.96	64.83	68.94	68.91	63.71	61.95	47.52	47.5	49.9	50.2	51.07	52.57	51.48	35.80	36.08
TiO_2	b.d.l.	b.d.l.	0.03	b.d.l.	b.d.l.	0.12	b.d.l.	0.01	0.19	1.59	0.30	0.91	2.12	6.47	1.35	3.96	3.55
ZrO_2	-	-	-	-	-	-	-	-		0.08	b.d.l.	0.03	1.27	0.09	0.04	-	-
Al_2O_3	18.58	18.25	18.37	18.95	18.51	18.95	22.55	23.37	4.29	1.91	0.16	0.49	0.23	0.21	0.30	12.49	13.11
FeO^T	0.43	0.23	0.03	0.08	1.45	0.94	0.11	0.26	24.05	32.6	33.2	34.8	27.49	24.94	27.80	25.40	25.97
MnO	b.d.l.	0.02	b.d.l.	0.02	b.d.l.	b.d.l.	0.06	0.00	0.28	0.74	0.80	0.57	0.29	0.28	0.94	0.29	0.42
ZnO	-	-	-		-	-	-	-	0.06	0.21	0.41	0.28	0.13	0.08	0.31	0.05	0.00
MgO	-	-	-	b.d.l.	-	-	-	b.d.l.	7.98	0.69	0.05	0.33	0.13	b.d.l.	0.05	7.53	6.87
CaO	b.d.l.	b.d.l.	0.04	0.18			4.16	4.79	11.46	4.45	0.01	0.33	4.80	0.46	0.29	0.03	0.03
BaO	b.d.l.	b.d.l.	0.38	0.22	-	b.d.l.	-	b.d.l.	-	-	-	-	-	-	-	0.15	0.08
SrO	b.d.l.	b.d.l.	-	-	-	-	-	-	-	-	-	-	-	-	-	-	-
Na_2O	4.92	0.21	3.22	4.66	10.55	11.84	8.04	8.59	0.98	5.46	7.65	6.64	10.35	12.77	13.04	0.10	0.07
K_2O	9.70	16.79	11.85	10.08	0.07	0.05	0.60	0.91	0.59	1.43	3.76	1.81	b.d.l.	b.d.l.	b.d.l.	9.11	9.55
F	-	-	-	-	-	-	-	-	0.71	0.50	0.92	0.37	-	-	-	0.63	0.73
Cl	-	-	-	-	-	-	-	-	0.11	0.03	b.d.l.	b.d.l.	-	-	-	0.33	0.36
H_2O	-	-	-	-	-	-	-	-		-	-	-	-	-	-	3.57	3.57
Total	100.15	100.05	98.88	99.04	99.70	100.96	99.23	99.905	98.20	96.89	97.39	96.79	97.87	97.88	95.59	99.43	100.39
O=(F,Cl)	-	-	-	-	-	-	-	-	*0.32*	*0.22*	*0.39*	*0.16*	-	-	-	*0.96*	*1.10*

and Vlach 2007b). As expected from the *subsolvus* character of these rocks, the integrated alkali-feldspar compositions are richer in the Or molecule when compared to those of the Papanduva Pluton. Almost pure albite is also seen interstitial to alkali feldspar crystals and as partial rims on sodic plagioclase in plagioclase-alkali feldspar contacts.

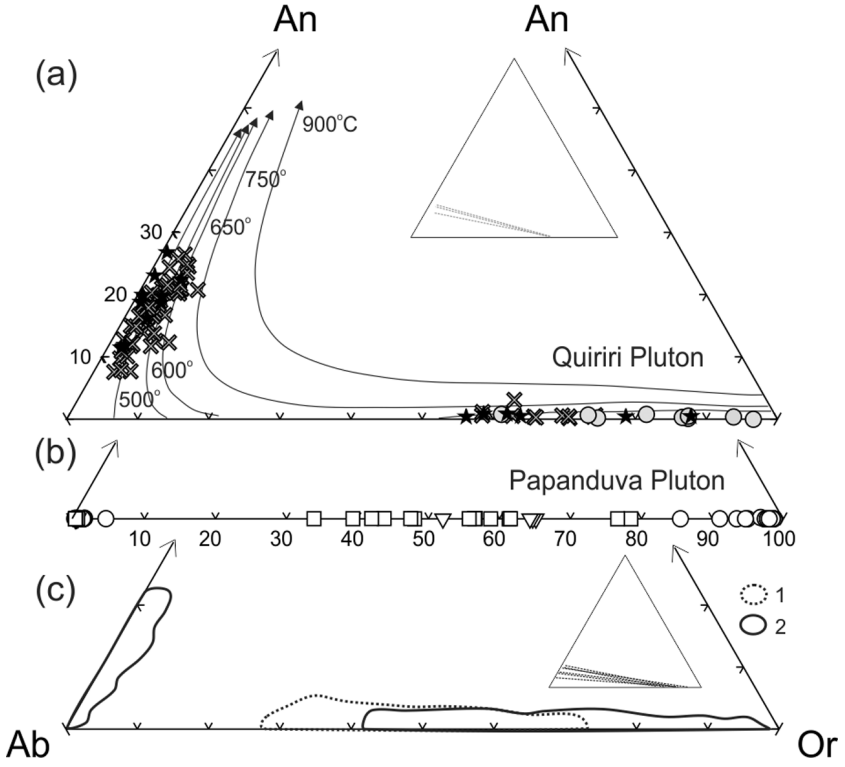

Figure 9 - Average compositions of core, intermediate zone and rim for alkali feldspar and albite, and individual chemical analysis of plagioclase in the An-Ab-Or molecular ternary plot for representative samples of the Quiriri **(a)** and Papanduva **(b)** Plutons. Available chemical data for feldspars from other plutons of the Graciosa Province are shown for comparison **(c)**: plutons of the alkaline **(1)** and aluminous **(2)** associations in the Serra da Graciosa region (Gualda and Vlach 2007b). Solvus curves for Ptotal = 100 MPa, according to the model after Fuhrman and Lindsley (1988). Inset ternary plots in **(a)** and **(c)** show compositions of coexistent plagioclase and alkali feldspar crystals. Symbols as in Fig. 5.

Plagioclase

Primary sodic plagioclase occurs in the Quiriri Pluton as isolated euhedral to subhedral tabular crystals, sometimes in aggregates of 2 to 4 grains, often with post-magmatic partial albite rims and sericitic and saussuritic alterations at different intensities. They correspond to oligoclase, with compositions around $Ab_{73-87}An_{24-11}Or_{2-8}$ and normal to slightly oscillatory compositional zoning (Table I, Fig. 9). On the other hand, plagioclase from both felsic microgranular and leucocratic medium to fine-grained enclaves shows more calcic compositions, up to sodic-andesine (An_{30-35}), as qualitatively verified under the microscope.

Amphiboles

Sodic-calcic and sodic amphiboles are the main mafic phases in the Papanduva peralkaline granites. They appear as isolated interstitial crystals, in aggregates of 3-4 grains or as elongated deformed

megacrysts in the deformed 'protomylonitic' facies. Most crystals display concentric to irregular patchy compositional zoning. Na-Ca amphibole (ferrorichterite) is found only in the massive facies, whilst sodic varieties are ubiquitous and correspond to both arfvedsonite and riebeckite, the latter being typical of the deformed 'cataclastic' and microgranitic facies. Compositional variations are defined by increasing Si, Fe^{3+}, Na and K and decreasing Al, Fe^{2+} and Ca contents from core to crystal rims. However, these variations do not span a wide compositional range as observed in other plutons of the Graciosa Province, since Ca-richer compositions are absent (Table I, Fig. 10a).

Ca-amphiboles occur only in samples from the grayish Q2 facies of the Quiriri Pluton. They form rare, isolated, euhedral crystals partially replaced by chlorite, epidote, magnetite and fluorite. In some cases, only pseudomorphosed crystals are seen. Compositions correspond to ferrohornblende, edenite, and ferro-edenite, with Na contents (up to 2.4 wt. % Na_2O) higher than those registered in similar plutons of the province (Gualda and Vlach 2007c). Zoning is very discrete, with some increasing in Na and K and decreasing in Ca and Al contents towards crystal rims (Table I, Fig. 10a).

Clinopyroxenes

Clinopyroxenes appear in samples of the Papanduva Pluton as interstitial yellow-greenish isolated crystals and in aggregates of several prismatic and/or fibrous grains. They comprise both late and post-magmatic phases and often appear as mantles around amphiboles. Concentric, patchy and irregular compositional zoning are common features. Some samples from the massive and deformed 'protomylonitic' facies present two other textural generations of pyroxene, recognized by their contrasted pleochroic schemes, one with dark-green, and another with orange to yellow pleochroic colors. The former is replaced by a yellow-greenish clinopyroxene whereas the latter appears as mantles around both phases in the deformed 'protomylonitic' facies.

The widespread yellow-greenish clinopyroxene corresponds to an aegirine or titanian aegirine ($Aeg_{81-99}Jd_{5-0}WEF_{15-0}$), with up to 7.0 wt. % TiO_2. The dark-green variety is an aegirine-augite ($Aeg_{72-80}Jd_1WEF_{27-18}$) and the orange-yellowish phase corresponds to an almost pure aegirine ($Aeg_{93-97}Jd_{3-1}WEF_{5-2}$) with relatively high Mn contents (up to 0.97 wt. % MnO, cf. Table I). The main compositional trend is defined by increasing Na and Fe^{3+} and decreasing Ca and Fe^{2+} contents from crystal cores to rims, in a relatively narrow range. Compositions plot along the Na (Aeg) – Fe^{2+}+Mn (Hd) axis in the ternary plot Na (Aeg) x Mg (Di) x Fe^{2+}+Mn (Hd) of Fig. 10b, most of them close to the Na (Aeg) apex, a compositional trait that highly contrasts with the observed evolutional trends in the whole Graciosa Province, marked by an initial decrease in Mg and increase in Fe^{2+} + Mn, followed by a moderate increase in Na contents (Fig. 10b). Therefore, clinopyroxenes from the Papanduva Pluton correspond to the most evolved compositions observed elsewhere within the province, with high Na (9.7 – 13.6 wt. % Na_2O) and negligible Mg (lower than 0.2 wt. % MgO) contents.

Biotite

Biotite is the typical mafic mineral in samples from the Quiriri Pluton. It occurs as interstitial crystals with orange to brownish pleochroism. Compositions are nearly homogeneous, with Fe/(Fe+Mg) cationic ratios and Al^{IV} varying between 0.56 – 0.70 and 2.1 – 2.5, respectively (Table I, Fig. 10c). Crystals in the mafic microgranular enclaves are slightly more magnesian, with Fe/(Fe+Mg) ratios between 0.47 and 0.61. Most compositions are equivalent to those commonly registered in biotites from anorogenic alkaline suites (cf. Abdel-Rahman 1994). They partially overlap the compositions of biotite in plutons of the Serra da Graciosa Region (Gualda and Vlach 2007b) and

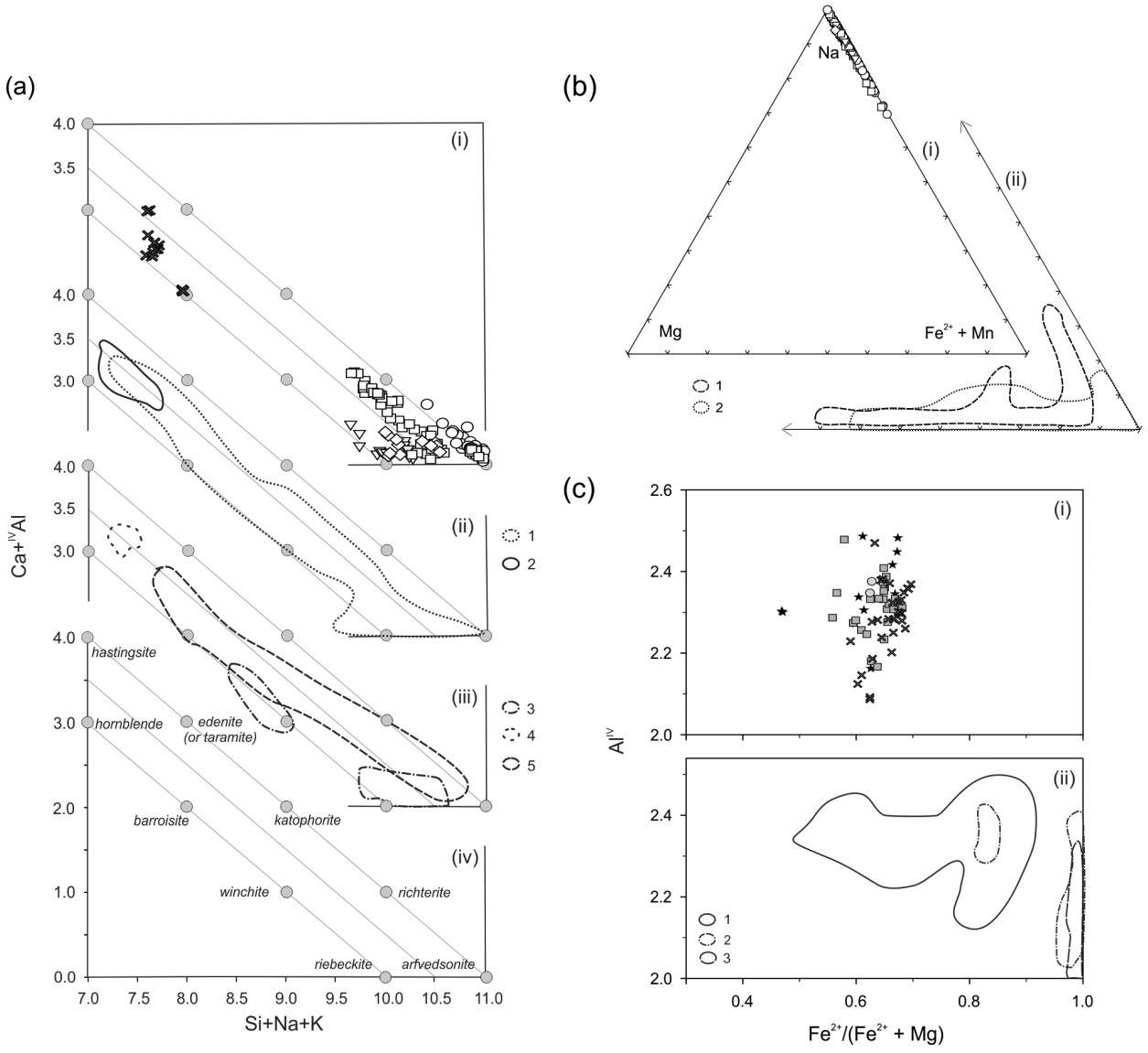

Figure 10 - Compositional variation diagrams for the main mafic minerals in the Papanduva and Quiriri Plutons, Morro Redondo Complex. **(a)** (Si + Na + K) vs. (Ca + ^{IV}Al) cationic plots showing the compositional evolution of amphiboles from the Morro Redondo Complex (i). In (ii) and (iii), compositional trends registered for other plutons from the Graciosa Province are portrayed for comparison: 1, Serra da Graciosa Plutons, alkaline association (Gualda and Vlach 2007b, c); 2, Serra da Graciosa Plutons, aluminous association (Gualda and Vlach 2007b, 2007c); 3, Mandira Massif, alkaline association (Santos and Vlach 2010); 4, Mandira Massif, aluminous association (Santos and Vlach 2010); 5, Corupá Pluton, alkaline association (Garin 2003). Nomenclature of ideal amphibole end-members are shown in (iv). End-members with the A position completely vacant fall along the lower line; end-members with the A position completely filled fall along the upper line. **(b)** Na–Mg–(Fe^{2+} + Mn) cationic plots showing the compositions of clinopyroxenes in the Papanduva Pluton (i). In (ii) compositional trends observed in other plutons from the alkaline association in the Graciosa Province are shown: 1, Corupá Pluton (Garin 2003); 2, Serra da Graciosa Plutons (Gualda and Vlach 2007b). **(c)** ^{IV}Al vs. Fe/(Fe+Mg) cationic plots for biotite of Quiriri Pluton (i). In (ii), compositional trends for other aluminous occurrences from the Graciosa Province are drawn for comparision: 1, Serra da Graciosa Plutons (Gualda and Vlach 2007b); 2, Mandira Massif (Santos and Vlach 2010); 3, Desemborque (Guaraú) Pluton (R.P. Garcia and S.R.F. Vlach unpublished data). Symbols as in Fig. 5.

are more magnesian than biotite from the Mandira (Santos and Vlach 2010) and Guaraú Massifs (R.P. Garcia and S.R.F. Vlach, unpublished data) from the Graciosa Province (Fig. 10c).

A remarkable compositional feature of the studied biotite, as well as from most occurrences in the province, is that it does not follow the *Fe-avoidance* model of Muñoz (1984), and variable positive correlations are observed between F and Fe contents. In fact, the calculated X_F and X_{Mg} molar fractions, when plotted against each other, define a field in which this model does not play a major role (Mason 1992, Charoy and Raimbault 1994).

Whole-Rock Geochemistry

Major and trace-element compositions of representative granite samples of Papanduva and Quiriri plutons, for which a complete FRX and ICP data set is available, are presented in Table II. Additional data may be requested from the first author. Moreover, some previous data are also presented by Kaul and Cordani (2000) for granites and Góis (1995) for granites and volcanic rocks. In the latter, an alkaline nature for the rhyolites, with varieties of both comendites and panterellerites, and a calc-alkaline to alkaline nature for basalts, andesi-basalts and andesites were pointed out.

TABLE II

Representative whole-rock chemical data of granites of the Papanduva and Quiriri Plutons, Morro Redondo Complex. Oxides and elements are given in wt. % and ppm, respectively. (*) FRX analyses, others ICP-MS analyses. LOI = lost on ignition, fe# = $FeO^T/(FeO^T+MgO)$, oxide wt. %; AI (Agpaitic Index) = $(Na_2O+K_2O)/Al_2O_3$ and ASI (Alumina Saturation Index) = $Al_2O_3/(CaO+Na_2O+K_2O)$ in moles; Tsat(zr) and Tsat(ap) = zircon and apatite saturation temperatures (°C, nc = not calculated); A = Radiogenic heat production per volume unit (μWm^{-3})

Plutons	Papanduva								
Facies	Massive				Protomyl.			Catacl.	Microgranitic
Sample	MR-215	MR-62	MR 32	MR 39	MR 03	MR 02	MR 21	MR 01A	MR 01D
SiO_2	74.53	75.40	76.04	75.91	74.55	75.38	77.78	75.98	73.99
TiO_2	0.179	0.224	0.137	0.219	0.163	0.161	0.086	0.211	0.109
Al_2O_3	11.30	11.33	10.79	11.52	9.89	10.58	11.25	10.83	11.34
$Fe_2O_3^T$	3.09	2.85	3.65	2.91	5.62	3.85	1.77	2.91	3.75
MnO	0.046	0.051	0.045	0.042	0.084	0.059	0.030	0.060	0.054
MgO	0.05	0.10	0.03	0.07	0.03	0.03	0.02	0.01	0.03
CaO	0.28	0.35	0.21	0.20	0.15	0.23	0.13	0.26	0.26
Na_2O	4.58	4.21	4.97	4.14	5.24	4.68	4.22	4.34	4.65
K_2O	4.69	4.71	4.08	4.74	3.77	4.33	4.75	4.66	4.69
P_2O_5	0.012	0.015	0.007	0.016	0.007	0.008	0.008	0.009	0.004
LOI	0.20	0.20	0.48	0.50	0.34	0.32	0.22	0.44	0.30
Total	98.96	99.44	100.44	100.27	99.84	99.63	100.26	99.71	99.18
fe#	0.982	0.962	0.991	0.974	0.994	0.991	0.988	0.996	0.991
ASI	0.861	0.895	0.832	0.936	0.762	0.826	0.913	0.856	0.859
AI	1.116	1.061	1.167	1.037	1.284	1.171	1.074	1.125	1.122
Li	38.6	31.8	65.1	30.0	178.6	73.2	24.7	29.7	84.4
Be	7.93	6.57	8.34	5.87	9.40	11.0	6.41	7.90	5.72
Sc	0.71	0.94	0.89	1.42	1.52	1.33	0.56	1.17	0.50
Zn*	135	114	200	114	347	199	89	147	158
Ga*	32	29	32	28	36	33	32	30	38
Rb	130	123	151	104	302	195	147	136	132
Sr	11.0	16.0	5.68	5.46	4.77	4.92	1.66	5.22	2.32
Y	170	112	303	71.4	323	165	145	168	59.8

TABLE II (continuation)

Pluton	Papanduva								
Facies	Massive				Protomyl.			Catacl.	Micrograniticc
Sample	MR-215	MR-62	MR 32	MR 39	MR 03	MR 02	MR 21	MR 01A	MR 01D
Zr*	776	781	1174	708	2428	1798	748	1217	523
Nb	48.0	45.6	55.8	44.3	88.1	52.4	21.3	65.5	21.5
Cs	9.39	0.76	0.64	0.40	1.25	1.34	0.51	1.61	0.59
Ba	83.7	144	20.9	81.0	16.2	28.5	4.22	40.0	4.57
La	104	188	168	90.3	119	94.1	200	164	31.3
Ce	231	297	237	123	233	177	268	274	63
Pr	24.4	34.6	41.9	18.1	30.1	21.8	32.4	32.5	8.79
Nd	91.1	120	180	63.9	119	82.8	113	120	35.3
Sm	21.1	23.6	51.2	11.9	31.8	20.1	21.7	26.1	8.96
Eu	0.92	1.07	2.14	0.55	1.34	0.80	0.76	1.01	0.32
Gd	21.4	20.6	56.3	10.6	39.1	21.7	20.5	26.2	9.35
Tb	3.63	3.23	8.77	1.76	6.78	3.78	3.05	4.46	1.50
Dy	21.8	18.7	50.0	11.3	43.0	24.3	17.5	28.2	9.27
Ho	4.54	3.78	9.48	2.46	9.19	5.27	3.44	5.93	1.95
Er	12.5	10.6	23.5	7.68	26.1	15.7	9.49	17.1	5.92
Tm	1.81	1.53	2.91	1.20	3.73	2.31	1.31	2.48	0.95
Yb	11.6	10.1	17.9	8.55	24.1	15.4	8.40	15.9	7.37
Lu	1.57	1.41	2.58	1.30	3.46	2.29	1.22	2.21	1.27
Hf	22.1	19.6	31.2	19.8	61.2	46.4	19.4	33.7	13.1
Pb	42.7	24.1	61.5	18.3	88.3	39.5	21.2	50.1	12.6
Th	32.4	26.9	37.9	26.1	47.9	32.4	22.2	42.1	11.4
U	3.70	3.28	4.85	2.89	7.81	6.20	2.01	4.43	1.27
Tsat(zr)	nc	nc	nc	nc	nc	nc	nc	nc	nc
Tsat(ap)	nc	nc	nc	nc	nc	nc	nc	nc	nc
A	3.6	3.1	4.3	3.0	5.7	4.2	2.5	4.5	1.6

Pluton	Quiriri										
Facies	Q1							Q2			Enclave
Sample	MR-161	MR-164	MR-202	MR-178	MR-174	MR-17	MR-201A	MR-193	MR-185	MR-186A	MR-201B
SiO_2	75.74	75.06	75.37	75.37	74.90	74.40	75.06	75.21	75.38	75.41	72.12
TiO_2	0.178	0.196	0.183	0.178	0.191	0.184	0.201	0.189	0.202	0.193	0.353
Al_2O_3	12.59	12.67	12.54	12.53	12.91	12.63	12.66	12.60	12.44	12.92	13.77
$Fe_2O_3^T$	1.47	1.47	1.37	1.37	1.40	1.39	1.50	1.43	1.51	1.03	2.59
MnO	0.027	0.026	0.021	0.023	0.025	0.025	0.023	0.028	0.033	0.016	0.061
MgO	0.14	0.16	0.15	0.14	0.16	0.16	0.20	0.19	0.16	0.12	0.49
CaO	0.53	0.69	0.66	0.64	0.68	0.62	0.70	0.69	0.63	0.59	1.08
Na_2O	3.52	3.43	3.46	3.42	3.44	3.54	3.53	3.46	3.46	3.47	3.85
K_2O	5.10	5.13	5.15	5.15	5.27	5.20	5.16	5.15	5.11	5.27	4.91
P_2O_5	0.021	0.026	0.021	0.022	0.024	0.019	0.027	0.023	0.024	0.024	0.075
LOI	0.44	0.46	0.42	0.46	0.52	0.52	0.46	0.34	0.46	0.58	0.30
Total	99.76	99.32	99.35	99.30	99.52	98.69	99.52	99.31	99.41	99.62	99.60
fe#	0.904	0.892	0.891	0.898	0.887	0.886	0.871	0.871	0.894	0.885	0.826
ASI	1.026	1.018	1.006	1.013	1.025	1.004	1.000	1.006	1.006	1.035	1.012
AI	0.898	0.884	0.898	0.894	0.880	0.907	0.900	0.894	0.902	0.883	0.846

TABLE II (continuation)

Pluton	Quiriri										
Facies	Q1							Q2			Enclave
Sample	MR-161	MR-164	MR-202	MR-178	MR-174	MR-17	MR-201A	MR-193	MR-185	MR-186A	MR-201B
Li	11.5	17.7	7.98	10.1	13.6	4.22	22.4	22.1	8.02	26.0	36.4
Be	3.04	3.35	3.36	5.57	3.53	2.79	4.28	3.24	3.78	3.35	7.98
Sc	1.96	2.07	1.93	1.86	2.12	1.77	2.08	1.90	1.87	2.04	3.43
Zn*	29	25	24	22	26	35	24	25	46	31	61
Ga*	18	19	19	19	20	19	20	19	19	18	19
Rb	138	132	134	137	155	138	136	130	135	143	164
Sr	57.7	61.3	56.6	54.9	60.1	53.1	56.4	54.9	55.3	52.0	71.8
Y	45.6	45.5	48.3	42.8	125	61.7	43.8	48.9	40.7	88.9	53.4
Zr*	170	183	176	167	176	179	178	183	174	182	300
Nb	20.8	22.0	20.5	18.3	19.3	19.0	23.2	21.3	17.3	21.5	25.6
Cs	1.13	1.38	1.02	1.26	1.46	1.44	1.51	1.54	1.27	1.46	2.26
Ba	647	712	648	640	710	693	700	624	651	694	902
La	73.9	74.2	70.4	66.7	285	87.7	71.7	71.8	73.9	215	74.5
Ce	148	150	144	112	423	172	117	148	145	251	154
Pr	13.3	13.5	13.0	12.4	45.5	16.3	13.2	13.4	13.5	34.0	14.4
Nd	43.1	44.6	42.1	40.3	146	54.2	43.6	43.8	44.1	109	49.2
Sm	7.68	8.18	7.55	7.37	25.8	10.2	8.04	7.97	7.83	19.1	9.32
Eu	0.62	0.71	0.62	0.66	1.61	0.81	0.72	0.64	0.67	1.58	0.95
Gd	7.01	7.47	6.97	6.78	21.9	9.58	7.42	7.23	6.75	15.3	8.26
Tb	1.16	1.21	1.17	1.11	3.26	1.59	1.18	1.21	1.07	2.25	1.34
Dy	7.00	7.07	7.13	6.66	18.4	9.57	6.94	7.29	6.24	12.5	7.93
Ho	1.49	1.48	1.56	1.43	3.65	2.05	1.45	1.55	1.32	2.46	1.68
Er	4.44	4.22	4.60	4.09	9.92	5.83	4.21	4.51	3.77	6.86	4.91
Tm	0.66	0.61	0.67	0.61	1.38	0.86	0.63	0.68	0.55	0.98	0.75
Yb	4.48	4.13	4.52	4.07	8.88	5.55	4.25	4.57	3.66	6.49	5.20
Lu	0.65	0.59	0.66	0.59	1.21	0.78	0.62	0.67	0.53	0.91	0.74
Hf	5.72	5.84	5.47	6.53	6.39	5.85	7.42	6.87	5.80	6.67	8.25
Pb	30.8	24.1	27.2	23.5	25.9	36.4	23.5	26.0	40.8	27.6	37.6
Th	24.5	24.4	23.5	23.0	30.5	25.1	28.0	24.1	22.5	25.9	26.6
U	3.94	2.73	2.94	2.56	3.34	2.25	2.78	2.54	3.15	3.91	4.90
Tsat(zr)	797	802	798	794	799	799	798	801	797	804	843
Tsat(ap)	821	832	817	821	824	800	835	823	828	828	897
A	3.2	2.9	2.9	2.7	3.5	2.8	3.1	2.8	2.8	3.3	3.6

Co, Cr and Ni below detection limits.

Most of the major and trace-element geochemical signatures of the granites from Morro Redondo Complex are typical of A-type or intraplate granites from other occurrences in the Graciosa Province and elsewhere (Collins et al. 1982, Pitcher 1993, Whalen et al. 1987, Vlach and Gualda 2007, Nardi and Bitencourt 2009, Frost and Frost 2011). They are alkali-rich ($8.7 \leq Na_2O + K_2O \leq 9.3$ wt. %), ferroan (Frost et al. 2001, Frost and Frost 2011) evolved rocks that exhibit a narrow compositional range, with $74 \leq SiO_2 \leq 78$ wt. %. In the normative haplogranitic Or-Ab-Qz ternary (Fig. 11), built according to the projection scheme of Blundy and Cashman (2001) to consider An-bearing compositions, these rocks plot close to the granitic minimum at considerably low pressures.

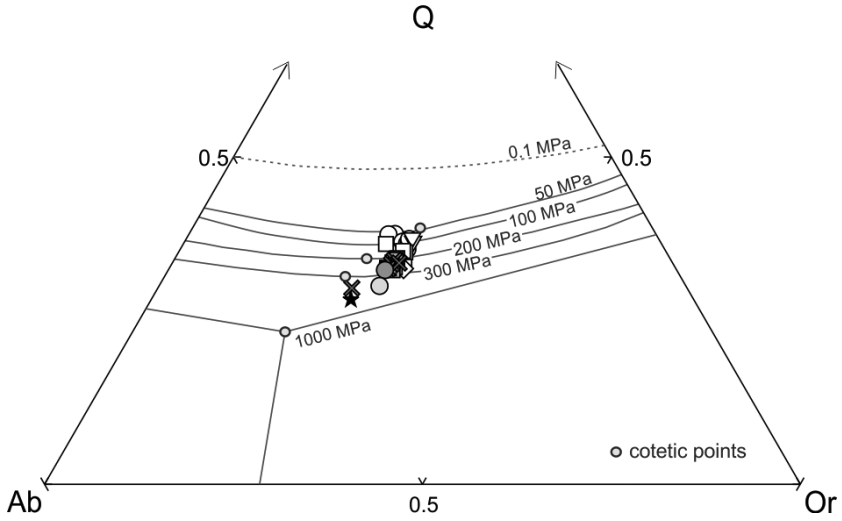

Figure 11 - Normative compositions for selected samples of the Quiriri and Papanduva Plutons in the haplogranitic Or-Ab-Qz ternary system. Units are weight fractions. Silica-feldspar cotetics from Blundy and Cashman (2001). Symbols as in Fig 5.

The ternary also depicts the relatively Qz-poor and plagioclase-rich nature of the aluminous samples from the Quiriri Pluton.

Selected geochemical diagrams are shown in Fig. 12 to emphasize the main contrasts between the alkaline and aluminous (subalkaline) granites. The fe# numbers are ≥ 0.96 and between 0.87 and 0.91, while molecular ASI (Alumina Saturation) and AI (Agpaitic) indexes vary between 0.76 – 0.94, 1.04 – 1.28 and 1.00 – 1.04, 0.88 – 0.91 in the peralkaline and in the main peraluminous granites from the Papanduva and Quiriri plutons, respectively. In the former, these indexes show a distinct larger range of variation, as well as a very good positive correlation. It is noteworthy that in the Quiriri Pluton, the hornblende-bearing granite (facies Q2), as well as the felsic enclave hosted in the main Q1 granites have lower fe# (0.82 and 0.83, respectively) and AI, while the granite porphyries (facies Q4) present fe# values similar to the peralkaline granites (0.99 – 1.00) as well as a somewhat higher AI. As expected, the peralkaline granites register lower CaO contents, as well as Al_2O_3/Fe_2O_3 and K_2O/Na_2O molecular ratios than the main aluminous ones. These ratios correlate positively in the peralkaline samples.

Typical chondrite-normalized trace-element patterns are displayed in Fig. 13. Compared with the Quiriri main peraluminous Q1 granites, which present relatively monotonous patterns, the Papanduva peralkaline granites are relatively enriched in the alkaline metals, Zn, Ga, Th, Nb, Zr, Hf, Y, M-HREE, and depleted in the alkaline-earth metals, P and Ti. The relative enrichment in HFSEs of the peralkaline granites is significant, with Zr, Nb, Y, REE^T abundances of up to 2430, 88, 320 and 996 ppm, respectively. In the Quiriri Pluton, the felsic enclave, with lower fe#, as well as the granite porphyries, with higher fe#, tend to present greater incompatible element abundances. Correlations between selected trace elements contents with the Agpaitic Index are depicted in Fig. 14. This plot reinforces the findings reported above and, of importance, depicts the wide variation range and the well-marked positive correlation of most of the LIL and HFS elements with AI as registered in the chemical signature of the peralkaline granites.

Total REE+Y contents vary between ca. 250 and 1150 ppm and are between ca. 1 and 3 orders of magnitude higher than those for chondrite (Fig. 15). When compared to the peralkaline Papanduva

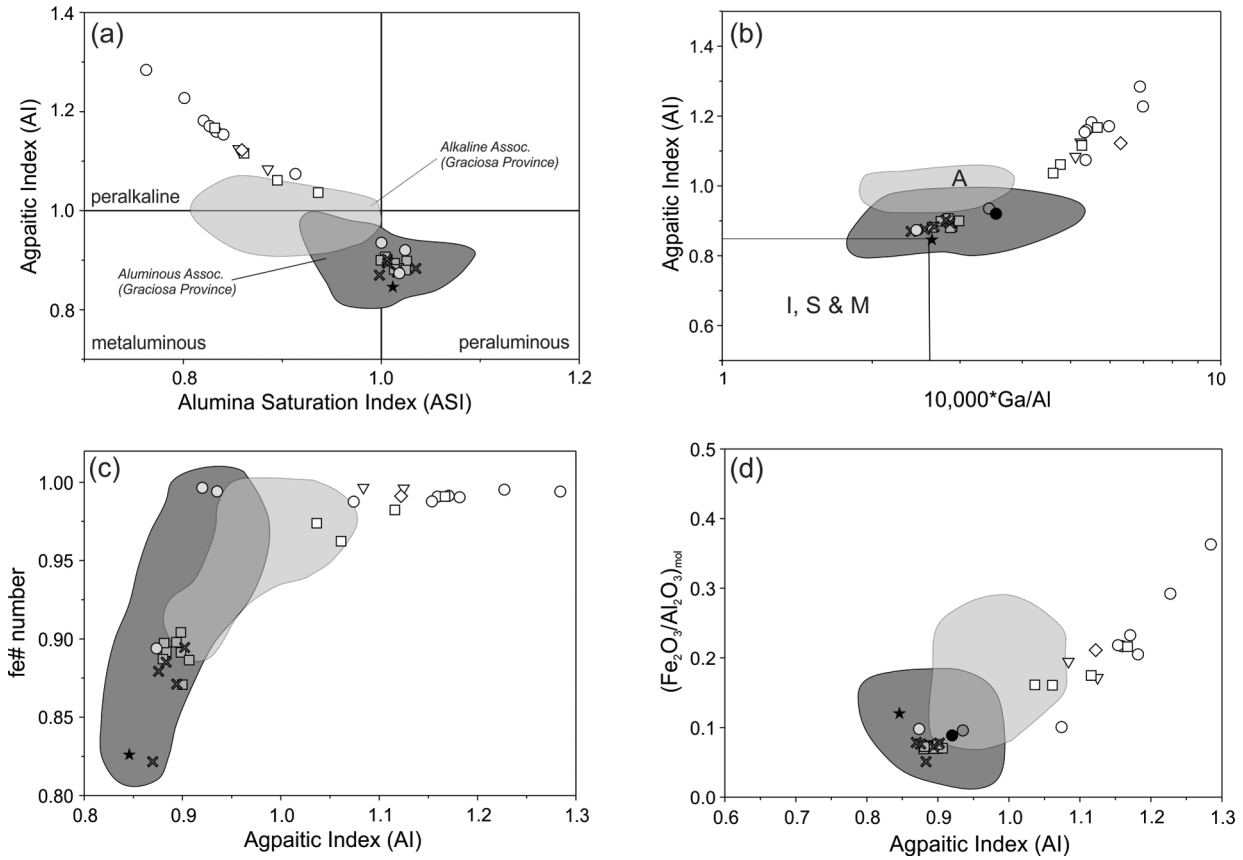

Figure 12 - Discriminating chemical diagrams for representative samples, highlighting compositional contrasts among the aluminous and peralkaline granites from the Quiriri and Papanduva Plutons, respectively. Available data for other occurrences from the province (Gualda and Vlach 2007a, 2007b, and references therein) are shown in gray fields for comparisons. (a) Alumina Saturation Index [ASI = Al_2O_3/(CaO+Na_2O+K_2O) mol] *vs.* Agpaitic Index [AI = (Na_2O+K_2O)/Al_2O_3 mol]. (b) 10^4*Ga/Al (Whalen et al. 1987) *vs.* AI; labels indicate I-, S-, M- and A-type granite fields. (c) AI *vs.* fe# number [= FeOt/(FeOt + MgO), wt.%]. (d) AI *vs.* $Fe_2O_3{}^T/Al_2O_3$ molecular ratios. Note the positive linear correlations between ASI, Ga/Al and $Fe_2O_3{}^T/Al_2O_3$ with AI. Symbols as in Fig. 5.

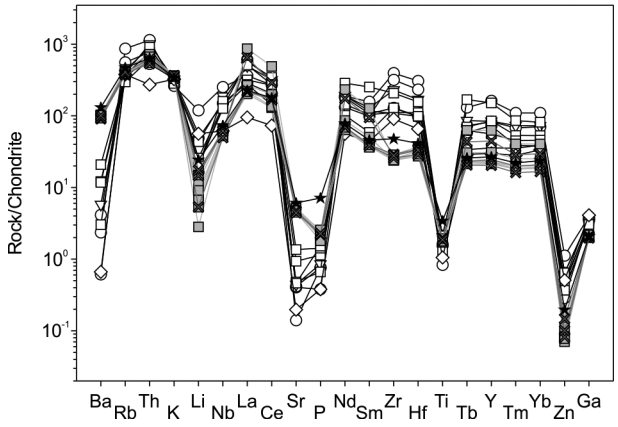

Figure 13 - Chondrite-normalized multi-element diagram showing relative enrichment and depletion patterns for selected samples from the Quiriri and Papanduva plutons, Morro Redondo Complex. Normalizing factors after Thompson (1982), plus Li, Zn and Ga after McDonough and Sun (1995). Symbols as in Fig. 5.

granites, the patterns for the main peraluminous Quiriri granites show a higher fractionation of the LREE over HREE and within the LREEs and the HREEs, with La_N/Yb_N, La_N/Nd_N and Dy_N/Lu_N ratios between 10 – 22 and 3 – 16, 3.1 – 3.8 and 1.7 – 3.5 and 1.1 – 1.5 and 0.7 – 1.9, respectively. Eu negative anomalies are a typical feature in all the investigated samples, with Eu/Eu* [Eu* = $(Sm_N*Gd_N)^{0.5}$] between 0.11 – 0.15 and 0.21 – 0.28 for the Papanduva and Quiriri plutons, respectively.

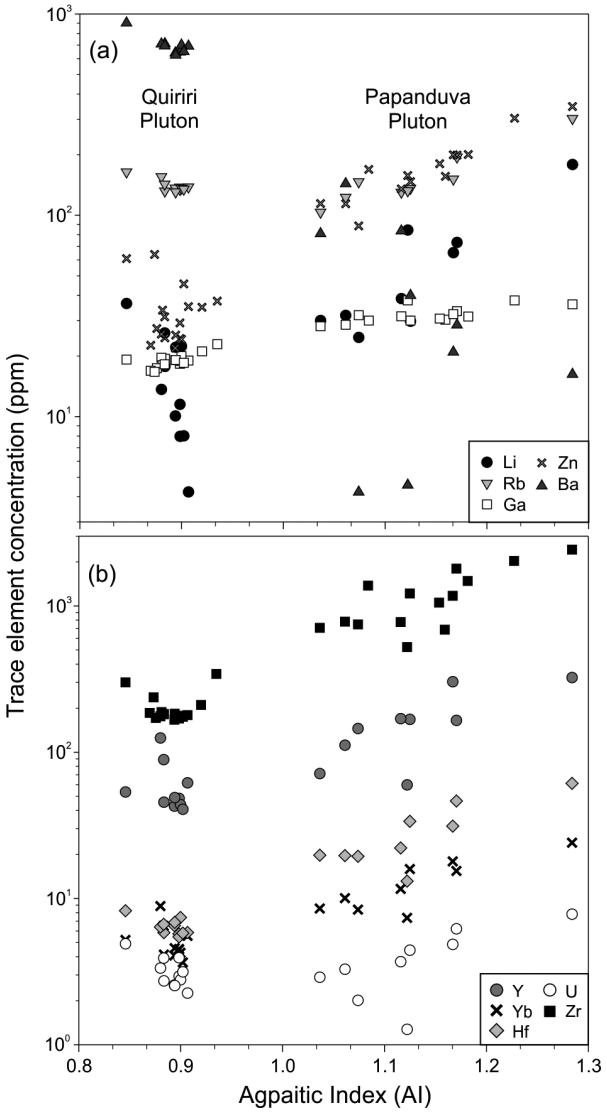

Figure 14 - Variation diagrams showing the behavior of selected LIL (a) and HFS (b) elements vs. AI for samples of the Quiriri and Papanduva Plutons, Morro Redondo Complex.

Altogether, geochemical signatures of the Quiriri Pluton are very akin with other peraluminous rocks from the aluminous association in the Graciosa Province (e.g. Gualda and Vlach 2007a, Vlach and Gualda 2007, cf. Fig. 12). However, with the exception of the felsic enclave, rocks with SiO_2 < 74.4 wt. % are lacking in this pluton (cf. Table II). On the other hand, the peralkaline alkali-feldspar granites of the Papanduva Pluton include the most evolved peralkaline rocks that constitute the alkaline association in the province.

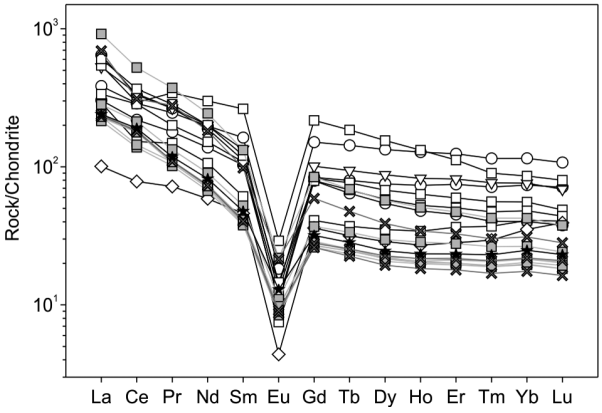

Figure 15 - Chondrite-normalized REE patterns for selected samples of the Quiriri and Papanduva Plutons, Morro Redondo Complex. Normalizing factors after Boynton (1984). Symbols as in Fig. 5.

Radiogenic Heat Production

Radiogenic heat is generated by the decay of radioactive isotopes ^{40}K, ^{232}Th, ^{235}U and ^{238}U and is directly related to the chemical and thermal evolution of the crust (e.g. Jaupart and Mareschal 1999, 2010, Bea 2012). Heat energy enhances hydrothermal circulation and high heat producing (HHP) granites are often associated with ore deposits and geothermal anomalies. Representative heat productions per unit volume (**A**) due to intrusive rocks of the Morro Redondo Complex are presented in Table II.

Heat production per volume (**A**) varies from 1.6 to 5.7 μWm^{-3} with a mean of ~3.3 μWm^{-3} (Fig. 16). The peralkaline Papanduva granites show both minimum and maximum values, and a

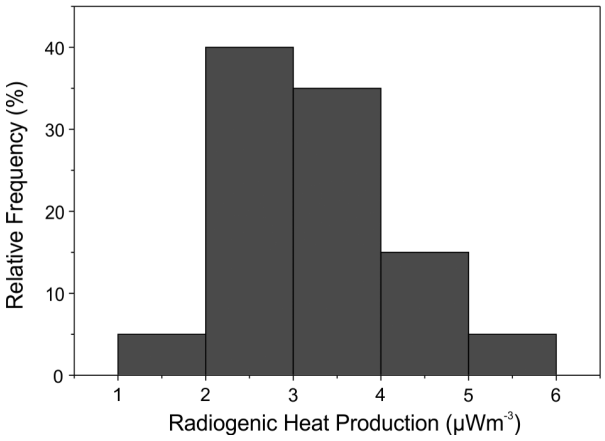

Figure 16 - Histogram showing typical values for the radiogenic heat production (**A**) for selected samples from the Quiriri and Papanduva plutons, Morro Redondo Complex.

higher mean (3.6 μWm^{-3}) when compared to the Quiriri granites, with a narrow range of variation (2.6 – 3.5 μWm^{-3}) and a mean of ~3.0 μWm^{-3}. The felsic microgranular enclave hosted by the main Quiriri granite gives 3.6 μWm^{-3}. These rates are much higher than (1) the typical values for upper and middle crusts (ca. 1.7 and 1.0 μWm^{-3}), (2) the average values registered in common granites and rhyolites (ca. 2.5 μWm^{-3}, cf. Rybach 1988, Haenel et al. 1988, Kemp and Hawkesworth 2003), and (3) those calculated for other occurrences within the province (our unpublished data). The highest **A** values computed for the Papanduva deformed 'protomylonitic' and 'cataclastic' facies (4.2 – 5.7 μWm^{-3}, mean of ~4.7 μWm^{-3}) approach those most typical of HHP granites elsewhere (e.g. Singh and Vallinayagam 2012).

Crystallization Conditions

The quantification of intensive parameters related to the emplacement and crystallization of the magmas that formed the A-type granites of the Morro Redondo Complex, and the Graciosa Province as a whole, is not an easy task, due to the lack of appropriate mineral assemblages, compositions and/or the intense late to post-magmatic transformations (e.g. Vlach and Gualda 2007, Anderson et al. 2008). Notwithstanding, a qualitative assessment may be drawn, as detailed below.

Lithostatic Pressure and Temperatures

Gualda and Vlach (2007a) emphasize that geological and petrographic evidences indicate that the emplacement of plutons from the Graciosa province are incompatible with confining pressures higher than ca. 200 MPa, an observation which is also in accordance with available gravimetric data (Hallinan et al. 1993). The scenario does not diverge for the Morro Redondo Complex, where the association of coeval plutonic and volcanic rocks, the presence of vugs, miarolitic cavities, volcanic xenoliths, as well as of granophyric inter-growths in the granites, point to crystallization in shallow crustal levels. Our Ab-Or-Qz normative data also supports this inference (Fig. 11).

The assemblage biotite + hornblende + titanite + Fe-Ti oxides (+ quartz + alkali feldspar + plagioclase) in samples from the Quiriri Pluton allows for the application of the geobarometer Al-in-hornblende of Anderson and Smith (1995), calibrated with the plagioclase-hornblende thermometry of Holland and Blundy (1994). Pressure estimates vary between 60 and 120 MPa, with a mean value of 80 (± 20) MPa (Fig. 17a), which seems to be a reasonable result, in agreement with estimated confining pressures for other shallow alkaline massifs and complexes elsewhere (e.g. Larsen and Sørensen 1987, Potter et al. 2004, Mann et al. 2006). However, this value may be underestimated, since plagioclase compositions in the Quiriri Pluton are relatively sodic (An_{8-27}) and so, the expected Al^{IV} contents in hornblende would be lower than those observed in calibrated experiments (Anderson and Smith 1995).

Zircon and apatite saturation temperatures were estimated for Quiriri samples following Watson and Harrison (1983, see also Hanchar and Watson 2003 and Miller et al. 2003) and Harrison and Watson 1984 (see also Pichavant et al. 1992). Results are presented in Table II. All samples are within the calibrated range specified by Miller et al.

(2003), with a *M* factor [= (Na+K+2Ca)/(Al·Si), in cations] between 1.36 and 1.46. Evaluated temperatures range from 794 to 860 °C, with a mean of 807 °C (Fig. 17b). Most samples gave temperatures close to 800 °C, a value significantly lower than temperature estimates obtained for similar plutons from the Graciosa Province (Gualda and Vlach 2007a) and A-type granites elsewhere (e.g. Poitrasson et al. 1995, King et al. 1997, King et al. 2001), in the range 850 – 900 °C. Apatite saturation temperatures are always higher (800 – 897 °C), with a mean of 834 °C. The felsic enclave has zircon and apatite saturation temperatures of 847 and 897 °C, respectively (Fig. 17b).

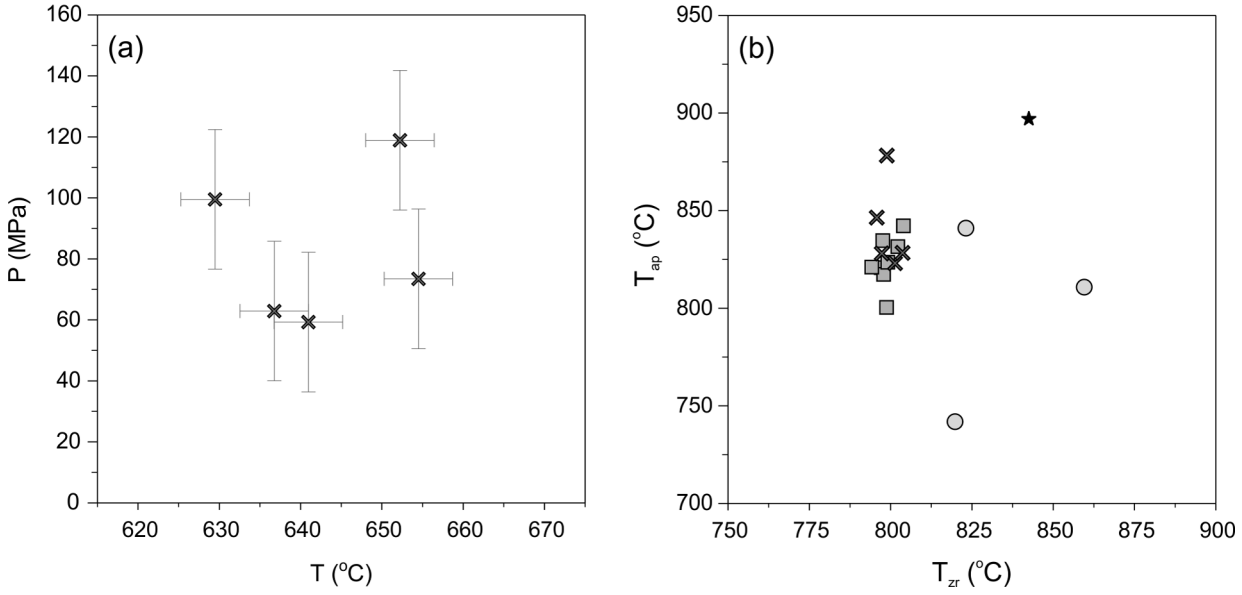

Figure 17 - Thermobarometric estimates for the Quiriri Pluton, Morro Redondo Complex. (a) Plagioclase-hornblende thermometry estimates (T in °C) of Holland and Blundy (1994) vs. Al-in-hornblende barometric estimates (P in MPa) of Anderson and Smith (1995). Uncertainty lines in T and P in each estimative represents 1σ precision error. (b) Zirconium-Saturation Thermometry estimates (T_{Zr}°C) of Watson and Harrison (1983) *vs.* Apatite Saturation Thermometry estimates (T_{ap}°C) of Harrison and Watson (1984). Symbols as in Fig 5.

Plagioclase-hornblende equilibrium temperatures were computed according to Holland and Blundy (1994), based on the reaction edenite + albite ↔ richterite + anorthite (see Anderson 1996). Estimated temperatures range from 629 to 655 °C, with a mean of ~643 (± 4) °C (Fig. 17a). They should be, however, interpreted with caution, given the high fe# values of Ca-amphiboles in the Quiriri Pluton, a feature that also prevents the use of the amphibole geothermometer of Ridolfi et al. (2010). Although qualitative, these temperatures estimates partially overlap those derived from the plagioclase – alkali feldspar solvus (500 – 650 °C, Fig. 9) and are consistent with the expected close-to-solidus temperatures in such granitic systems.

In peralkaline rocks like those from the Papanduva Pluton, any estimates of zircon or apatite saturation temperatures may result in meaningless values (e.g. Watson 1979, Keppler 1993, Miller et al. 2003). Although some authors argue that the crystallization of mineral phases such as Na-amphiboles and pyroxenes may allow magmas to turn saturated in Zr (cf. Watson 1979, Hanchar and Watson 2003), and others even consider zircon saturation temperatures as reasonable estimates (e.g. Shellnutt and Iizuka 2011), in peralkaline systems, even if zircon is a crystallizing phase and the *M* parameter is within the calibration range of Watson and Harrison (1983), Zr does not necessarily behave

as an essential structural trace element, since it may be also incorporated in significant amounts by other essential or accessory minerals. Furthermore, the positive correlation between AI and Zr contents in our samples indicates that Zr solubility increased with peralkalinity.Therefore, the calculated zircon saturation temperatures for zircon-bearing samples of the Papanduva Pluton (880 – 970 °C, mean ~930 °C) appear to be in disagreement with several evidences from peralkaline volcanic systems worldwide (cf. Macdonald 2012 and references therein); nevertheless they are not out of the expected range for some 'dry' A-type granites (e.g. Clemens et al. 1986, White et al. 2005).

Qualitative estimates of the solidus temperature for the Papanduva Pluton can be obtained from the mineral assemblage. Because of the presence of ferrorichterite and arfvedsonite, as well as aenigmatite as an important magmatic accessory phase, maximum solidus temperatures are suggested to fall within the interval between 700 – 750 °C (e.g. Ernst 1968, Thompson and Chisholm 1969, Scaillet and MacDonald 2001), which is in agreement with alkali feldspar solvus estimates, between 650 – 750 °C (Vilalva 2007).

Redox Conditions

Mineral assemblages and mafic silicate compositions observed in the Quiriri Pluton point to relatively oxidizing crystallization conditions. The paragenesis biotite ± Ca-amphibole + quartz + titanite + magnetite ± ilmenite indicates f_{O2} conditions close to or higher than the TMQAI [titanite – magnetite – quartz – amphibole (Fe-tremolite) – ilmenite] buffer (Noyes et al. 1983, Wones 1989), for which precise thermodynamic parameters were not well established yet. The fe# number [= Fe/(Fe + Mg), cations] of biotite and amphiboles leads to a similar conclusion. The equilibrium:

$$a_{\text{annite(Btss)}} + 0.5\ O_2 = a_{\text{sanidine (AFss)}} + a_{\text{magnetite (Mtss)}} + H_2O$$

where a stands for the activity of the indicated component in the main mineral solid solutions, was studied and calibrated by Wones (1981). It indicates that for a given f_{H2O}, the higher the oxidation state is, the lower the expected annite content within biotite will be, as the equilibrium will shift to the right. Similar reasoning can be applied to the fe# values observed in Ca-amphiboles (e.g. Anderson and Smith 1995). Using this equilibrium and a large data set including independent f_{O2} determinations and fe# numbers in biotite from magnetite-bearing Mesoproterozoic granites from Laurentia (USA), Anderson et al. (2008) estimated Δ_{QFM} values as a function of the biotite fe# number. Our compositions, mostly with $0.6 \leq$ fe# ≤ 0.7, give $\Delta_{QFM} \approx +1$, a value one or two units lower than the estimates based on the TMQAI equilibrium (Vlach and Gualda 2007). The fe# numbers measured in Ca-amphibole, down to 0.4, point also towards relatively high oxidizing conditions (Anderson and Smith 1995).

The stability of Na-Ca and Na-amphiboles in the peralkaline Papanduva granites suggest relatively reduced crystallization conditions, between the MW (Magnetite – Wüstite) and QFM (Quartz – Fayalite – Magnetite) buffers (Ernst 1968, Stolz 1986, Marks et al. 2003, Pe-Piper 2007). Such conditions turn progressively more oxidizing as crystallization proceeds and the occurrence of aenigmatite in an antipathetic relation with Fe-Ti oxides, a typical feature of several samples from the Papanduva Pluton, suggests crystallization inside the 'no-oxide field', an area in the T – fO_2 space where aenigmatite, aegirine and quartz coexist in the absence of Fe-Ti oxides, located above the QFM buffer in super-saturated rocks (Nicholls and Carmichael 1969, see also Vilalva 2007). Moreover, the relative stability of Na-amphiboles and aegirine depends on f_{O2}, f_{H2O}, and the availability of Na meta and di-silicates hypothetical molecules in the melt, as described by the equillibrium:

4 riebeckite + 4 (Na_2SiO_3) + 2 ($Na_2Si_2O_5$) + 3 O_2 = 20 aegirine + 4 H_2O

and a similar one relating aegirine to arfvedsonite (Bailey 1969, see also Deer et al. 1978). This reaction shows that in aenigmatite-absent rocks, the late to post-magmatic crystallization of aegirine, as isolated crystals or mantles around amphiboles, is favored in more oxidizing environments, limited by QFM and HM buffers (Bailey 1969, Vilalva 2007).

CONCLUSIONS AND FINAL REMARKS

The Morro Redondo Complex, one of the largest complexes in the Graciosa Province, is composed of high-SiO_2 rocks from the alkaline and aluminous associations of A-type granites that form two contrasting plutons namely Papanduva and Quiriri, as well as coeval acid and basic to intermediate volcanic rocks. Scarce field evidence suggests that granites were emplaced slightly after the volcanics, and at least some peralkaline rocks were emplaced after the main aluminous ones.

The Papanduva Pluton is made of *hypersolvus* aegirine ± arfvedsonite - alkali-feldspar granites with massive and deformational structures, the latter including 'cataclastic' and 'protomylonitic' facies, and low magnetic susceptibilities that formed in relatively reduced environments. Textural relationships between mafic and felsic minerals indicate that they followed an agpaitic crystallization sequence (e.g. Sørensen 1997, Andersen et al. 2010), in which main and accessory mafic phases appear after quartz and alkali feldspar.

The granites of the Papanduva Pluton are among the most evolved peralkaline rocks within the Graciosa Province, showing Agpaitic Indexes up to ca. 1.3, the highest Na and Fe^{3+} contents in Na-amphiboles and clinopyroxenes, as well as the highest LILE and HFSE abundances. These correlate positively with the peralkalinity grade (as measured by the Agpaitic Index), a geochemical signature that led to the crystallization of rare 'agpaitic' assemblages in the more evolved facies, as evidenced by the Ti-, Zr- and REE-rich unusual accessory mineralogy, formed during late to post-magmatic stages. It is worth mentioning that several among these minerals, including aenigmatite, neptunite, narsarsukite, Na-K zirconosilicates, nacareniobsite, turkestanite, as well as to date poorly studied and/or unidentified minor phases (Vilalva and Vlach 2010, Vilalva et al. 2013, Vlach and Vilalva 2007) are described for the first time in peralkaline granites from Brazil. Such mineralogical and textural features, along with geochemical data, indicate that the more evolved the liquids are, the higher the Agpaitic Index will be, as well as the Na_2O, $Fe_2O_3^T$, LILE and HFSE abundances.

The Quiriri Pluton has the largest area extent and comprises slightly peraluminous ($1.05 < ASI < 1.20$), *subsolvus* biotite ± hornblende syenogranites, as well as granite porphyries with higher magnetic susceptibilities, formed under relatively oxidizing conditions. Similar to other rocks of the aluminous association within the Graciosa Province (Gualda and Vlach 2007a, Vlach and Gualda 2007), Quiriri granites have homogeneous compositions, with relatively lower fe# numbers and $Fe_2O_3^T/Al_2O_3$ molecular ratios and higher Ca and alkaline earth metals, and are characterized by relatively Ca- and Al-rich mafic mineral paragenesis defined by annitic biotite ± hornblende + titanite ± allanite + magnetite + ilmenite + fluorite (+ apatite + zircon). Consequently, biotite and hornblende show discrete chemical variations, contrary to what is observed in amphiboles and clinopyroxenes from the peralkaline Papanduva granites. Furthermore, a remarkable feature of many samples from the Quiriri Pluton is the hydrothermal alteration which can be locally pervasive and in which some sulfides are seen.

Both plutons register relatively high heat productions. The highest **A** values (of up to 5.7 μWm^{-3}), are found in the deformed 'protomylonitic' granites of the Papanduva Pluton and approach those tipically found in HHP granites elsewhere. Such

characteristics reflect the geochemical signatures of the studied granites and are features mostly attributed to inheritance from their source rocks, enhanced later by magmatic fractionation processes.

Geological and petrographic evidence indicates that both plutons were emplaced at shallow crustal levels. Semi-quantitative pressure estimates for the hornblende-bearing Quiriri samples are about 100 MPa. Estimated close-to-liquidus zircon and apatite saturation temperatures for the Quiriri main granites vary between 800 and 850 °C, while for a felsic monzogranitic enclave within these rocks they range from ca. 850 to 900 °C, the higher values found through apatite saturation estimates. The presence of ubiquitous minute apatite inclusions in zircon crystals (F.C.J. Vilalva et al., unpublished data) suggest that this phosphate may be a liquidus phase, while zircon is coeval or slightly late. Altogether, these temperature estimates are somewhat lower than those observed in similar granites from the Serra da Graciosa region (Gualda and Vlach 2007a). Considering the close-to-solidus temperature calculated for the main Quiriri granites at ~650 °C, melts crystallization range was about 200 – 250 °C. Given the peralkaline nature of the Papanduva melts, it is difficult to attribute confidence to zircon saturation temperature estimates (up to 970 °C). Based on some data from alkaline rhyolite occurrences and laboratory experiments (Macdonald 2012, Scaillet and Macdonald 2001), we suggest a crystallization interval between ~800 and 600 °C for the peralkaline melts.

Ti-in-quartz temperatures (Wark and Watson 2006) in representative samples result in mean values of about 740 and 830 (± 20) °C for the main granites and felsic enclave from the Quiriri Pluton and 715 (± 20) °C for the Papanduva Pluton (our unpublished data). Except for the felsic monzogranitic enclave, such temperatures appear to be underestimated when compared with the saturation temperature estimates for the aluminous granites, as in fact, quartz was expected to be a relatively early crystallizing phase, considering the involved textures, rock compositions and emplacement pressures.

The peralkaline melts crystallized arguably under fO_2 conditions close to or slightly below the QFM buffer, some of them within the 'no-oxide' field of Nicholls and Carmichael (1969). Amphibole and clinopyroxene compositional variations, as well as the development of aegirine mantles around amphibole, indicate the crystallization followed an oxidizing path, ending close to the HM buffer in the post-magmatic stage, a common feature of most peralkaline occurrences in the Graciosa Province (e.g. Vlach and Gualda 2007). Conversely, melts that formed the Quiriri granites crystallized under more oxidizing conditions ($\Delta_{QFM} \geq 1$), close to the TMQAI buffer (Noyes et al. 1983, Wones, 1989), with evolution also following an oxidizing path.

ACKNOWLEDGMENTS

We would like to thank the agencies Fundação de Amparo à Pesquisa do Estado de São Paulo (FAPESP) (Proc. 08/00562-0) and Conselho Nacional de Desenvolvimento Científico e Tecnológico (CNPq) (Proc. 307583/2008-2) for financial support. F. Vilalva thanks the agencies Coordenação de Aperfeiçoamento de Pessoal de Nível Superior (CAPES) and CNPq (Proc. 142838/2007-1) for his Master and Doctoral scholarships. Comments by two anonymous referees helped improve the original manuscript and are very much appreciated.

RESUMO

O Complexo Morro Redondo é uma das ocorrências mais importantes da Província Graciosa de tipo-A, sul do Brasil. É constituído pelos plútons graníticos Papanduva e Quiriri e uma associação vulcânica bimodal contemporânea. O Plúton Papanduva inclui álcali-feldspato granitos peralcalinos maciços e deformados, com anfibólios e clinopiroxênios de Ca-Na e Na. Os tipos deformados são as rochas mais evoluídas na província e contêm minerais "agpaíticos" raros, alguns

sendo descritos pela primeira vez em granitos do Brasil. O Plúton Quiriri, maior, é constituído por biotita sieno- e monzogranitos levemente peraluminosos, maciços, com raro anfibólio de Ca. As composições da biotita são relativamente homogêneas, enquanto os anfibólios e piroxênios sódicos mostram trajetórias evolutivas de aumento de Na e Fe^{3+}. Os granitos Morro Redondo são ferroanos, com teores elevados de SiO_2, álcalis e HFSE; os tipos peralcalinos registrando os maiores valores de fe#. Os conteúdos de LILE e HFSE aumentam com o Índice Agpaítico e os mais evoluídos são granitos HHP, com produção de calor radiogênico de até 5.7 μWm^{-3}. Estimativas geotermobarométricas indicam colocação sob baixas pressões (~100 MPa), em temperaturas de até 850–800 °C, em ambientes relativamente reduzidos (QFM) e oxidantes ($+1 < \Delta_{QFM} < +3$) para os Plútons Papanduva e Quiriri, respectivamente. Em ambos os casos, os magmas evoluiram para condições mais oxidantes com o progresso da cristalização.

Palavras-chave: granitos de tipo-A, geoquímica, petrografia, Província Graciosa, mineralogia, complexo Morro Redondo.

REFERENCES

ALMEIDA RP, SANTOS MGM, FRAGOSO-CÉSAR ARS, JANIKIAN L AND FAMBRINI GL. 2012. Recurring extensional and strike-slip tectonics after the Neoproterozoic collisional events in the Southern Mantiqueira province. An Acad Bras Cienc 84: 347-376.

ABDEL-RAHMAN AFM. 1994. Nature of biotites from alkaline, calc-alkaline, and peraluminous magmas. J Petrol 35: 525-541.

ANDERSEN T, ERAMBERT M, LARSEN AO AND SELBEKK RS. 2010. Petrology of Nepheline Syenite Pegmatites in the Oslo Rift, Norway: Zirconium Silicate Mineral Assemblages as Indicators of Alkalinity and Volatile Fugacity in Mildly Agpaitic Magma. J Petrol 51: 2303-2325.

ANDERSON JL. 1996. Status of thermobarometry in granitic batholiths. Trans R Soc Edimburgh (Earth Sciences) 87: 125-138.

ANDERSON JL, BARTH AP, WOODEN JL AND MAZDAB F. 2008. Thermometers and Thermobarometers in Granitic Systems. Rev Mineral Geochem 69: 121-142.

ANDERSON JL AND SMITH DR. 1995. The effect of temperature and oxygen fugacity on Al-in-hornblende barometry. Am Mineral 80: 549-559.

BAILEY DK. 1969. The stability of acmite in the presence of H_2O. Am J Sci 267-A: 1-16.

BASEI MAS, SIGA JR O, MACHIAVELLI A AND MANCINI F. 1992. Evolução tectônica dos terrenos entre os Cinturões Ribeira e Dom Feliciano (PR-SC). Rev Bras Geociênc 22: 216-221.

BASTIN GF AND HEIJLIGERS HJM. 1990. Progress in electron-probe microanalysis. Materialwiss Werkst 21: 90-92.

BEA F. 2012. The sources of energy for crustal melting and the geochemistry of heat-producing elements. Lithos, 153: 278-291.

BLENKINSOP T. 2000. Deformation Microstructures and Mechanisms in Minerals and Rocks, Dordrecht: Kluwer Academic Publishers, 150 p.

BLUNDY J AND CASHMAN K. 2001. Magma ascent and crystallization at Mount St. Helens, 1980-1986. Contrib Mineral Petrol 140: 631-650.

BONIN B. 2007. A-type granites and related rocks: Evolution of a concept, problems and prospects. Lithos 97: 1-29.

BOYNTON WV. 1984. Cosmochemistry of the rare earth elements: meteorite studies. In: HENDERSON P (Ed), Rare earth element geochemistry, Amsterdan: Elsevier, p. 63-114.

CHAROY B AND RAIMBAULT L. 1994. Zr-, Th-, and REE-rich biotite differentiates in the A-type granite pluton of Suzhou (Eastern China): the key role of fluorine. J Petrol 35: 919-962.

CLEMENS JD, HOLLOWAY JR AND WHITE AJR. 1986. Origin of an A-type granite: experimental constraints. Am Mineral 71: 317-324.

COLLINS BJ, BEAMS SD, WHITE AJR AND CHAPPEL BW. 1982. Nature and origin of A-type granites with particular reference to southeastern Australia. Contrib Mineral Petrol 80: 189-200.

COUTINHO JMV. 2008. Dyke Swarms of the Paraná Triple Junction, Southern Brazil. Geol USP Sér Cient 8: 29-52.

DEER WA, HOWIE RA AND ZUSSMAN J. 1978. Rock-Forming Minerals. Volume 2A. Single-Chain Silicates, 2nd ed., London: Longman, 668 p.

DEER WA, HOWIE RA AND ZUSSMAN MA. 1992. An introduction to the rock-forming minerals, 2nd ed., New York: Prentice Hall, 712 p.

DROOP GTR. 1987. A general equation for estimating Fe^{3+} in ferromagnesian silicates and oxides from microprobe analysis, using stoichiometric criteria. Mineral Mag 51: 431-437.

EBY GN. 1992. Chemical subdivision of the A-type granitoids: petrogenetic and tectonic implications. Geology 20: 641-644.

ERNST WG. 1968. Amphiboles. Crystal Chemistry, phase relations and occurrence, New York: Springer-Verlag, 128 p.

FROST BR, BARNES CG, COLLINS WJ, ARCULUS RJ AND FROST CD. 2001. A geochemical classification for granitic rocks. J Petrol 42: 2033-2048.

FROST CD AND FROST BR. 2011. On ferroan (A-type) granites: their compositional variability and modes of origin. J Petrol 52: 39-53.

FUHRMAN ML AND LINDSLEY DH. 1988. Ternary-feldspar modeling and thermometry. Am Mineral 73: 201-215.

GERASIMOVSKY VI, VOLKOV VP, KOGARKO LN AND POLYAKOV AI. 1974. Kola Peninsula. In: SØRENSEN H (Ed), The Alkaline Rocks, New York: J Willey & Sons, p. 206-220.

GÓIS JR. 1995. Contribuição à petrografia e geoquímica da parte setentrional do complexo vulcano-plutônico Morro Redondo, divisa do Paraná com Santa Catarina. Unpublished MSc Dissertation, Universidade de São Paulo, SP, Brazil, 86 p.

GUALDA GAR AND VLACH SRF. 2005. Stoichiometry-based estimates of ferric iron in calcic, sodic-calcic and sodic amphiboles: a comparison of various methods. An Acad Bras Cienc 77: 521-534.

GUALDA GAR AND VLACH SRF. 2007a. The Serra da Graciosa A-type Granites and Syenites, southern Brazil. Part 1: Regional setting and geological characterization. An Acad Bras Cienc 79: 405-430.

GUALDA GAR AND VLACH SRF. 2007b. The Serra da Graciosa A-type Granites and Syenites, southern Brazil. Part 2: Petrographic and mineralogical evolution of the alkaline and aluminous associations. Lithos 93: 310-327.

GUALDA GAR AND VLACH SRF. 2007c. The Serra da Graciosa A-type Granites and Syenites, southern Brazil Part 3: Magmatic evolution and post-magmatic breakdown of amphiboles of the alkaline association. Lithos 93: 328-339.

HAENEL R, RYBACH L AND STEGENA L. 1988. Handbook of terrestrial heat-flow density determination, Dordrecht: Kluwer Academical Publishers, 486 p.

HALLINAN SE, MANTOVANI MSM, SHUKOWSKY W AND BRAGGION JR I. 1993. Estrutura do escudo Sul-Brasileiro: uma revisão através de dados gravimétricos e magnetométricos. Rev Bras Geociênc 23: 201-214.

HANCHAR JM AND WATSON EB. 2003. Zircon saturation thermometry. Rev Mineral Geochem 53: 89-112.

HARRISON TM AND WATSON EB. 1984. The behavior of apatite during crustal anatexis - equilibrium and kinetic considerations. Geochim Cosmochim Acta 48: 1467-1477.

HOLLAND Y AND BLUNDY J. 1994. Non-ideal interactions in calcic amphiboles and their bearing on amphibole-plagioclase thermometry. Contrib Mineral Petrol 116: 433-447.

ISSC. 1987. Stratigraphic classification and nomenclature of igneous and metamorphic rock bodies. GSA Bull 99: 440-442.

JAUPART C AND MARESCHAL JC. 1999. The thermal structure and thickness of continental roots. Lithos 48: 93-114.

JAUPART C AND MARESCHAL JC. 2010. Heat Generation and Transport in the Earth, Cambridge: Cambridge University Press, 476 p.

KAUL PFT. 1984. Significado dos granitos anorogênicos da suíte intrusiva Serra do Mar na evolução da crosta no sul-sudeste do Brasil, no âmbito das folhas SG.22-Curitiba e SG.23-Iguape. In: CONGRESSO BRASILEIRO DE GEOLOGIA 33, Rio de Janeiro, RJ, Brasil. Anais 6: 2815-2825.

KAUL PFT. 1997. O magmatismo na Serra do Mar e adjacências (Sul do Brasil) no final do Neoproterozóico e seus condicionantes tectônicos. Unpublished PhD Thesis, Universidade de São Paulo, SP, Brazil, 293 p.

KAUL PFT AND CORDANI UG. 1994. Aspectos petrográficos, geoquímicos geocronológicos dos Maciços Graníticos da Serra do Mar no Leste paranaense e vizinhanças. In: CONGRESSO BRASILEIR DE GEOLOGIA 38, Camboriú, SC, Brazil, Anais 2: 371-373.

KAUL PFT AND CORDANI UG. 2000. Geochemistry of the Serra do Mar granitoid magmatism and tectonic implications, southern Brazil. Rev Bras Geociênc 30: 115-119.

KEMP AIS AND HAWKESWORTH CJ. 2003. Granitic perspectives on the generation and secular evolution of the continental crust. In: RUDNICK R (Ed), Treatise On Geochemistry 12: The Crust, Oxford: Elsevier Science, p 349-410.

KEPPLER H. 1993. Influence of fluorine on the enrichment of high field strength trace elements in granitic rocks. Contrib Mineral Petrol 111: 113-121.

KING PL, CHAPPELL BW, ALLEN CM AND WHITE AJR. 2001. Are A-type granites the high-temperature felsic granites? Evidence from fractionated granites of the Wangrah Suite. Aust J Earth Sci 48: 501-514.

KING PL, WHITE AJR, CHAPPEL BW AND ALLEN CM. 1997. Characterization and origin of aluminous A-type granites from the Lachland fold belt, southeastern Australia. J Petrol 38: 371-391.

LAMEYRE J. AND BOWDEN P. 1982. Plutonic rock type series: discrimination of various granitoid series and related rocks. J Volcanol Geoth Res 14: 169-189.

LARSEN LM AND SØRENSEN H. 1987. The Ilímaussaq intrusion - progressive crystallization and formation of layering in an agpaitic magma. In: FITTON JG AND UPTON BGJ (Eds), Alkaline Igneous Rocks, London: The Geological Society, p 437-488.

LEAKE BE ET AL. 1997. Nomenclature of amphiboles: report of the Subcommittee on Amphiboles of The International Mineralogical Association Commission on New Minerals and Mineral Names. Can Mineral 35: 219-246.

LEAKE BE ET AL. 2004. Nomenclature of amphiboles: Additions and revisions to the International Mineralogical Association's Amphibole Nomenclature. 2004. Am Mineral 89: 883-887.

LIÉGEOIS JP. 1998. Preface – Some words on the postcollisional magmatism. Lithos 45: xv-xvii.

LITVINOVSKY BA, JAHN B, ZANVILEVICH AN, SAUNDERS A, POULAIN S, KUZMIN DV, REICHOW MK AND TITOV AV. 2002. Petrogenesis of syenite–granite suites from the Bryansky Complex (Transbaikalia, Russia): implications for the origin of A-type granitoid magmas. Chem Geol 189: 105-133.

MAACK R. 1953. Mapa Geológico do Estado do Paraná. Escala 1:750.000. Ed. da Comissão de Comemorações do Centenário do Paraná (1853-1953). Curitiba: Governo do Paraná.

MACDONALD R. 2012. Evolution of peralkaline silicic complexes: Lessons from the extrusive rocks. Lithos 152: 11-22.

MACHADO R., GÓIS JR, PLÁ CID J AND CONCEIÇÃO H. 1993. Maciço alcalino de Morro Redondo (Paraná): abordagem petrográfica das fácies vulcânica e plutônica. In: REUNIÃO ANUAL DA SBPC 45, Recife, PE, Brasil, Atas 1: p. 632.

MANN U, MARKS M AND MARKL G. 2006. Influence of oxygen fugacity on mineral compositions in peralkaline melts: The Katzenbuckel volcano, Southwest Germany. Lithos 91: 262-285.

MARKS M, VENNEMANN T, SIEBEL W AND MARKL G. 2003. Quantification of magmatic and hydrothermal processes in a peralkaline syenite–alkali granite complex based on textures, phase equilibria, and stable and radiogenic isotopes. J Petrol 44: 1247-1280.

MARTIN RF. 2006. A-type granites of crustal origin ultimately result from open-system fenitization-type reactions in an extensional environment. Lithos 91: 125-136.

MASON RA. 1992. Models of order and iron-fluorine avoidance in biotite. Can Mineral 30: 343-354.

MCDONOUGH WF AND SUN S-S. 1995. The Composition of the Earth. Chem Geol 120: 223-253.

MILLER CF, MCDOWELL SM AND MAPES RW. 2003. Hot and cold granites? Implications of zircon saturation temperatures and preservation of inheritance. Geology 31: 529-532.

MORI PE, REEVES S, CORREIA CT AND HAUKKA M. 1999. Development of a fused glass disc XRF facility and comparision with the pressed powder pellet technique at Instituto de Geociências, São Paulo University. Rev Bras Geociênc 29: 441-446.

MORIMOTO NJ, FABRIES J, FERGUSON AK, GINZBURG IV, ROSS M, SEIFERT FA, ZUSSMAN J, AOKI K AND GOTTARDI G. 1988. Nomenclature of pyroxenes. Am Mineral 73: 1123-1133.

MUÑOZ JL. 1984. F-OH and Cl-OH exchange in micas with applications to hydrothermal ore deposits. Rev Mineral 13: 469-493.

NARDI LVS AND BITENCOURT MF. 2009. A-type granitoids in post-collisional settings from southernmost Brazil: their classification and relationship with magmatic series. Can Min 47: 1493-1504.

NAVARRO MS, ANDRADE S, ULBRICH HHGJ, GOMES CB AND GIRARDI VAV. 2008. The direct determination of rare earth elements in basaltic and related rocks using ICP-MS: Testing the efficiency of microwave oven sample decomposition procedures. Geost Geoanal Res 32: 167-180.

NICHOLLS J AND CARMICHAEL ISE. 1969. Peralkaline acid liquids: a petrological study. Contrib Mineral Petrol 20: 268-294.

NOYES HJ, WONES DR AND FREY FA. 1983. A tale of two plutons: petrographic and mineralogic constraints on the petrogenesis of the Red Lake and Eagle Peak plutons, central Sierra Nevada, California. J Geol 91: 487-509.

PASSCHIER CW AND TROUW RAJ. 2005. Microtectonics. 2nd ed., Berlin Heidelberg: Springer-Verlag, 366 p.

PE-PIPER G. 2007. Relationship of amphibole composition to host-rock geochemistry: the A-type gabbro-granite Wentworth pluton, Cobequid shear zone, eastern Canada. Eur J Mineral 19: 29-38.

PICHAVANT M, MONTEL JM AND RICHARD LR. 1992. Apatite solubility in peraluminous liquids: Experimental data and an extension of the Harrison-Watson model. Geochim Cosmochim Acta 56: 3855-3861.

PITCHER WS. 1993. The Nature and Origin of Granite, London: Blackie Academic and Professional, 321 p.

POITRASSON E, DUTHOU JL AND PIN C. 1995. The relationship between petrology and Nd isotopes as evidence for contrasting anorogenic granite genesis: Example of the Corsican Province (SE France). J Petrol 36: 1251-1274.

POTTER J, RANKIN AH AND TRELOAR PJ. 2004. Abiogenic Fischer-Tropsch synthesis of hydrocarbons in alkaline igneous rocks; fluid inclusion, textural and isotopic evidence from the Lovozero complex, N.W. Russia. Lithos 75: 311-330.

PRAZERES FILHO HJ, HARARA OM, BASEI MAS, PASSARELLI CR AND SIGA JR O. 2003. Litoquímica, Geocronologia U-Pb e Geologia Isotópica (Sr-Nd-Pb) das Rochas Graníticas dos Batólitos Cunhaporanga e Três Córregos na Porção Sul do Cinturão Ribeira, Estado do Paraná. Geol USP Sér Cient 3: 51-70.

PUTNIS A, HINRICHS R, PUTNIS CV, GOLLA-SCHINDLER U AND COLLINS LG. 2007. Hematite in porous red-clouded feldspars: evidence of large-scale crustal fluid-rock interaction. Lithos 95: 10-18.

QIU JS, WANG DZ, MCINNES BIA, JIANG SY, WANG RC AND KANISAWA S. 2004. Two subgroups of A-type granites in the coastal area of Zhejiang and Fujian Provinces, SE Cina: age and geochemical constraints on their petrogenesis. Trans Roy Soc of Edin-Earth Sci 95: 227-236.

RIDOLFI F, RENZULLI A AND PUERINI M. 2010. Stability and chemical equilibrium of amphibole in calc-alkaline magmas: an overview, new thermobarometric formulations and application to subduction-related volcanoes. Contrib Mineral Petrol 160: 45-66.

RYBACH L. 1988. Determination or heat production rate. In: Handbook of terrestrial-flow density determinations. In: HAENEL R, RYBACH L AND STEGENA L (Eds), Kluwer Academic Publishers, Dordrecht, p. 125-142.

SANTOS CA AND VLACH SRF. 2010. Variações composicionais em anfibólios e biotita de granitos do Maciço Mandira, Província Graciosa de Granitos e Sienitos de Tipo (A). In: CONGRESSO BRASILEIRO DE GEOLOGIA 45, Belém, PA, Brasil, Anais (CD).

SCAILLET B. AND MACDONALD R. 2001. Phase relations of peralkaline silicic magmas and petrogenetic implications. J Petrol 42: 825-845.

SCHMITT AK, EMMERMANN R, TRUMBULL RB, BÜHN B AND HENJES-KUNST F. 2000. Petrogenesis and $^{40}Ar/^{39}Ar$ geochronology of the Brandberg Complex, Namibia: evidence for a major mantle contribution in metaluminous and peralkaline granites. J Petrol 41: 1207-1239.

SCHUMACHER JC. 1997. Appendix 2, the estimate of ferric iron in electron microprobe analysis of amphiboles. Can Mineral 35: 238-246.

SHELLNUTT JG AND IIZUKA Y. 2011. Mineralogy from three peralkaline granitic plutons of the Late Permian Emeishan large igneous province (SW China): evidence for contrasting magmatic conditions of A-type granitoids. Eur J Mineral 23: 45-61.

SIGA JR O, BASEI MAS, REIS NETO JM AND BUBA RM. 1994. Maciços graníticos da porção sudeste do Paraná e nordeste de Santa Catarina: geocronologia e implicações tectônicas. In: CONGRESSO BRASILEIRO DE GEOLOGIA 38, Camboriú, SC, Brasil, Anais 2: 400-401.

SIGA JR O, BASEI MAS, REIS NETO JM, MACHIAVELLI A AND HARARA OM. 1995. O Complexo Atuba: um cinturão Paleoproterozóico intensamente retrabalhado no Neoproterozóico. Bol IG-USP Sér Cient 26: 69-98.

SIGA JR O, BASEI MAS, SATO K, CORDANI UG AND CITRONI SB. 2000. U-Pb and Sm-Nd isrotopic studies of Campo Alegre and Guaratubinha volcano-sedimentary basins, Southern region. In: INTERNATIONAL GEOLOGICAL CONGRESS 31, Rio de Janeiro, Brazil, Abstracts (CD).

SINGH L. AND VALLINAYAGAM G. 2012. High Heat Producing Volcano-Plutonic Rocks of the Siner Area, Malani Igneous Suite, Western Rajasthan, India. Int J Geosci 3: 1137-1141.

SØRENSEN H. 1997. The agpaitic rocks; an overview. Mineral Mag 61: 485-498.

STOLZ AJ. 1986. Mineralogy of the Nandewar Volcano, Northeastern New South Wales, Australia. Mineral Mag 50: 241-255.

STRECKEISEN A. 1976. To each plutonic rocks its proper name. Earth-Sci Rev 12: 1-33.

THOMPSON RN. 1982. Magmatism of the British Tertiary province. Scot J Geol 18: 49-107.

THOMPSON RN AND CHISHOLM JE. 1969. Synthesis of aenigmatite. Mineral Mag 37: 253-255.

TREIN E. 1967. Geologia da folha de Tijucas do Sul. Comissão da Carta Geológica do Paraná. BADEP-UFPR, Unpublished report. 36 p.

ULBRICH HHGJ, VLACH SRF AND JANASI VA. 2001. O mapeamento faciológico em rochas ígneas plutônicas. Rev Bras Geociênc 31: 163-172.

VILALVA FCJ. 2007. Petrografia e mineralogia de granitos peralcalinos: O Plúton Papanduva, Complexo Morro Redondo (PR/SC). Unpublished MSc Dissertation, Universidade de São Paulo, SP, Brasil, 289 p. Available online at http://www.teses.usp.br/teses/disponiveis/44/44143/tde-14122007-093212/en.php.

VILALVA FCJ AND VLACH SRF. 2009. Quimismo de ilmenita rica em Mn e Zn em granitos peralcalinos do Complexo Morro Redondo, PR-SC. In: CONGRESSO BRASILEIRO DE GEOQUÍMICA 12, Ouro Preto, MG, Brazil. Anais… (CD), SBGq.

VILALVA FCJ AND VLACH SRF. 2010. Major- and trace-element composition of *REE*-rich turkestanite from peralkaline granites of the Morro Redondo Complex, Graciosa Province, south Brazil. Mineral Mag 74: 645-658.

VILALVA FCJ, VLACH SRF AND SIMONETTI A. 2013. Nacareniobsite-(Ce) and britholite-(Ce) in peralkaline granites from the Morro Redondo Complex, Graciosa Province, Southern Brazil: occurrence and compositional data. Can Min 51: 313-332.

VLACH SRF AND GUALDA GAR. 2007. Allanite and chevkinite in A-type granites and syenites of the Graciosa Province, southern Brazil. Lithos 97: 98-121.

VLACH SRF, JANASI VA AND VASCONCELLOS ACBC. 1990. The Itu Belt: associated calc-alkaline and aluminous A-type late Brasiliano granitoids in the States of São Paulo and Paraná, Southern Brazil. In: CONGRESSO BRASILEIRO DE GEOLOGIA 36, Natal, RN, Brazil. Anais 4: 1700-1711.

VLACH SRF, SIGA JR O, HARARA OM, GUALDA GAR, BASEI MAS AND VILALVA FCJ. 2011. Crystallization ages of the A-type magmatism of the Graciosa Province (Southern Brazil): Constraints from zircon U-Pb (ID-TIMS) dating of coeval K-rich gabbro-dioritic rocks. J South Am Earth Sci 32: 407-415.

VLACH SRF AND VILALVA FCJ. 2007. Ocorrência de narsarsukita, britholita-(Ce) e nacareniobsita-(Ce) em granitos peralcalinos do Complexo Morro Redondo (PR/SC), Província Graciosa. In: CONGRESSO BRASILEIRO DE GEOQUÍMICA 11, Atibaia, SP, Brazil. Anais…(CD), SBGq.

WARK DA AND WATSON EB. 2006. TitaniQ: a titanium-in-quartz geothermometer. Contrib Mineral Petrol 152: 743-754.

WATSON EB. 1979. Zircon saturation in felsic liquids: experimental data and application to trace element geochemistry. Contrib Mineral Petrol 70: 407-419.

WATSON EB AND HARRISON TM. 1983. Zircon saturation revisited: temperature and composition effects in a variety of magma types. Earth Planet Sci Lett 64: 295-304.

WHALEN JB, CURIE KL AND CHAPPEL BW. 1987. A-type granites: Geochemical characteristics, discrimination and petrogenesis. Contrib Mineral Petrol 95: 407-419.

WHITE JC, REN M AND PARKER DF. 2005. Variation in mineralogy, temperature, and oxygen fugacity in a suite of strongly peralkaline lavas and tuffs, Pantelleria, Italy. Can Mineral 43: 1331-1347.

WONES DR 1981. Mafic silicates as indicators of intensive variables in granitic magmas. Min Geol 31: 191-212.

WONES DR. 1989. Significance of the assemblage titanite + magnetite + quartz in granitic rocks. Am Mineral 74: 744-749.